PHYSICAL REVIEW B, VOLUME 63, 245117

Antiferromagnetic phase in the Hubbard model by means of the composite operator method

Adolfo Avella* and Ferdinando Mancini
Dipartimento di Fisica ''E.R. Caianiello'' – Unità INFM di Salerno, Università degli Studi di Salerno, 84081 Baronissi (SA), Italy

Roland Münzner
Institut für Theoretische Physik, Universität Tübingen, Auf der Morgenstelle 14, 72 076 Tübingen, Germany

(Received 19 July 2000; revised manuscript received 16 January 2001; published 7 June 2001)

We have investigated the antiferromagnetic phase of two-dimensional (2D), three-dimensional (3D), and extended Hubbard models on a bipartite cubic lattice by means of the composite operator method within a two-pole approximation. This approach yields a fully self-consistent treatment of the antiferromagnetic state that respects the symmetry properties of both the model and the algebra. The complete phase diagram, as regards the antiferromagnetic and paramagnetic phases, has been drawn. We first reported, within a pole approximation, three kinds of transitions at half-filling: Mott-Hubbard, Mott-Heisenberg, and Heisenberg transitions. We have also found a metal-insulator transition, driven by doping, within the antiferromagnetic phase. This latter is restricted to a very small region near half-filling, and has, in contrast to what has been found by similar approaches, a finite critical Coulomb interaction as a lower bound at half-filling. Finally, it is worth noting that our antiferromagnetic gap has two independent components: one due to the antiferromagnetic correlations, and another coming from the Mott-Hubbard mechanism.

DOI: 10.1103/PhysRevB.63.245117 PACS number(s): 71.10.Fd, 71.27.+a, 75.10.−b

I. INTRODUCTION

For almost half a century, the Hubbard model[1] has been one of the fundamental models in a theoretical description of strongly correlated electron systems. Despite its simplicity, it has always been taken as one of the prototypes when modeling electrons in narrow bands. Within this context it had wide applications in the theory of magnetism[2–4] and metal-insulator transitions.[5] The discovery of the high-T_c superconducting cuprate materials,[6] where the special properties are to a large extent due to strong correlations,[7] put an impetus on the investigation of the Hubbard model and its derivates as the t-t'-U model, the extended Hubbard model, and the t-J model. To gain a better theoretical understanding of high-T_c materials, not only the superconducting phase of the proposed models is studied, but also their normal phase and those with further broken symmetries. The antiferromagnetic state is of particular interest, as it is believed that the pairing mechanism in the cuprates is mainly due to magnetic correlations in an itinerant electronic system. In addition, the high-T_c compounds show a wide range of metal-insulator transitions; in particular, a phase transition from an antiferromagnetic insulator to a superconductor is observed. The antiferromagnetic phase of the Hubbard model has been the subject of intensive study by both numerical and analytical methods.

Despite the simplicity of the model, there are no exact solutions known except for a few special cases,[3,8] and one must turn to approximate solutions. The dynamical mean-field theory (DMFT)[9] and a variety of projection techniques [10–18] are among the most popular approaches to the Hubbard model and its derivates.

The *composite operator method* (COM)[14,15,19] that we present here belongs to the above-mentioned class of projection techniques. Choosing a set of field operators built up from the electronic ones (hence the name) as elements of the fundamental spinor, the equation of motion for the Green's function of this spinor is obtained. This equation has been solved by means of both a pole approach[14,15] and a two-site resolvent method.[19] The use of composite operators requires a careful choice of the Fock space, where the Green's function is realized. We have shown that the Pauli principle plays a fundamental role in unambiguously fixing the representation by determining the parameters that appear in the scheme, owing to the noncanonical algebra of the composite operators.[20,21] Let us note that, by the Pauli principle, we mean all relations among operators dictated by the algebra. A comprehensive treatment of the paramagnetic phase of the Hubbard model within the two-pole approximation has led to a good agreement with both numerical studies and some experimental properties of the cuprates.[15,22] In the case of the one-dimensional (1D) Hubbard model we have shown that the two-pole approximation reproduces almost exactly the Bethe ansatz results for the ground-state energy.[23]

In the last years an intensive study by the spectral density approach (SDA)[11,12] of the magnetic phases of the Hubbard model on different lattice types and by varying dimensionality has been done,[24–26] and the complete magnetic phase diagram of the Hubbard model on a 3D fcc lattice was derived.[26] The SDA corresponds to an expansion of the Green's function in terms of the electronic spectral moments. It has been shown that this approach corresponds to the COM when a specific choice of the basic spinor is made and the pole approximation is used.[27] However, this correspondence is only relative to the functional dependence of the Green's function, and huge differences arise when the representation is not properly fixed.[28,21,20]

To complement the analysis of the paramagnetic phase for the Hubbard model in the two-pole approximation by the COM, we present here a study of the antiferromagnetic phase within this framework. As the most simple case of antiferromagnetism, where in general the spin and the translational invariance are broken, we consider an antiferromagnetic state on a bipartite lattice characterized by its staggered magnetization. It turns out that in this phase the simple Hubbard model does not provide sufficient internal parameters to fix the representation. We therefore investigate the t-t'-U model in the limit of $t' \rightarrow 0$ in two and three dimensions, and the extended Hubbard model in two dimensions.

In Secs. II and III, we develop the analytical background needed for the calculations. We find a closed set of self-consistent equations for the antiferromagnetic thermal equilibrium state, which respects the Pauli principle and the particle-hole symmetry. The numerical evaluation of these self-consistent equations is presented in Secs. IV and V. The complete phase diagrams considering the paramagnetic and the antiferromagnetic phase for both models and in different dimensionality are calculated, as well as the density of states and the quasiparticle dispersions. The main results of the paper are the following: the presence of three kinds of transitions (Mott-Hubbard, Mott-Heisenberg, and Heisenberg) at half-filling in the plane T-U; the existence of two components in the antiferromagnetic gap (one due to the antiferromagnetic correlations, and another coming from the Mott-Hubbard mechanism); a finite critical value of the Coulomb interaction for the Mott-Hubbard and Mott-Heisenberg transitions; the strong decay of the Néel temperature with doping; and a metal-insulator transition away from half-filling inside the antiferromagnetic phase.

II. HUBBARD MODEL WITHIN THE TWO-POLE APPROXIMATION

The Hamiltonian for the single-band Hubbard model[1] with chemical potential μ is defined by

$$H=\sum_{ij;\sigma} (t_{ij}-\mu\delta_{ij})c^{\dagger}_{\sigma}(i)c_{\sigma}(j)+U\sum_{i} n_{\uparrow}(i)n_{\downarrow}(i), \tag{2.1}$$

with $\sigma\in\{\uparrow,\downarrow\}$, and where the sum over the site indices i and j runs over the whole chemical lattice $\{\mathbf{R}_i\}$, which we consider to be of simple cubic type with lattice constant a. U is the on-site Coulomb interaction. The kinetic part of the Hamiltonian is given by the nearest-neighbor hopping. In d dimensions, the hopping matrix takes the form $t_{ij}=-2\,d\,t\,\alpha_{ij}=-2\,d\,t 1/N\Sigma_{\mathbf{k}}e^{i\mathbf{k}\cdot(\mathbf{R}_i-\mathbf{R}_j)}\alpha(\mathbf{k})$, with $\alpha(\mathbf{k})=(1/d)\Sigma_{l=1}^{d}\cos(k_l a)$.

In the framework of the COM, as basic fields we take the Hubbard operators $\xi_\sigma(i)=c_\sigma(i)[1-n_{\bar{\sigma}}(i)]$ and $\eta_\sigma(i)=c_\sigma(i)n_{\bar{\sigma}}(i)$, where $n_\sigma(i)=c^{\dagger}_\sigma(i)c_\sigma(i)$, describing the basic excitations $n(i)=0\leftrightarrow n(i)=1$ and $n(i)=1\leftrightarrow n(i)=2$ on the lattice site i, which are responsible for the leading contributions in the electronic density of states.[29] Let us define a four-component composite field at lattice site i,

$$\Psi(i,t)=\begin{pmatrix}\xi_{\uparrow}(i,t)\\ \eta_{\uparrow}(i,t)\\ \xi_{\downarrow}(i,t)\\ \eta_{\downarrow}(i,t)\end{pmatrix}, \tag{2.2}$$

where the variable t denotes the time translation of the operator under the Heisenberg dynamics generated by H. The Heisenberg equation of motion for this basic field Ψ may be split into a part that is linear in the basic field and a remaining nonlinear part

$$i\frac{\partial}{\partial t}\Psi(i,t)=J(i,t)=\sum_{j}\,\varepsilon(i,j)\Psi(j,t)+\delta J(i,t) \tag{2.3}$$

by projecting it on the basic field. Then, the matrix $\varepsilon(i,j)$ is fixed by

$$\varepsilon(i,j)=\sum_{l}\,\langle\{J(i,t),\Psi^{\dagger}(l,t)\}\rangle\langle\{\Psi(l,t),\Psi^{\dagger}(j,t)\}\rangle^{-1}, \tag{2.4}$$

where $\langle\cdot\rangle$ denotes the thermal average on the grand-canonical ensemble.

To simplify the notational effort, we introduce the so-called normalization matrix I and the so-called m matrix

$$I(i,j)=\langle\{\Psi(i,t),\Psi^{\dagger}(j,t)\}\rangle, \tag{2.5}$$

$$m(i,j)=\langle\{J(i,t),\Psi^{\dagger}(j,t)\}\rangle, \tag{2.6}$$

and obtain the shorthand for the energy matrix $\varepsilon=mI^{-1}$ from Eq. (2.4).

The pole approximation consists of neglecting the nonlinear part $\delta J(i,t)$ in the equation of motion. This is equivalent to suppressing of the incoherent part in the retarded Green's function matrix

$$\begin{aligned}S(i,j,t)&=\theta(t)\langle\{\Psi(i,t),\Psi^{\dagger}(j,0)\}\rangle\\ &=\frac{i}{2\pi}\left(\frac{a}{2\pi}\right)^{d}\int d\omega e^{-i\omega t}\int_{\Omega_B}d^{d}k e^{i\mathbf{k}\cdot(\mathbf{R}_i-\mathbf{R}_j)}\\ &\quad\times\int_{\Omega_B}d^{d}p e^{i\mathbf{p}\cdot\mathbf{R}_i}S(\mathbf{k},\mathbf{p},\omega),\end{aligned} \tag{2.7}$$

which then satisfies the linearized equation of motion

$$i\frac{\partial}{\partial t}S(i,j,t)=i\delta(t)I(i,j)+\sum_{l}\,\varepsilon(i,l)S(l,j,t). \tag{2.8}$$

d is the dimension of the system, a is the lattice spacing, and Ω_B is the Brillouin zone. The resulting set of algebraic equations for the Fourier transform of the retarded Green's function may then be solved. A knowledge of the retarded Green's function will allow us to calculate the correlation functions $\langle\Psi(i,t)\Psi^{\dagger}(j,0)\rangle$ by means of the spectral theorem. As already mentioned, the above scheme of truncating the equation of motion by a projection technique is rather common in the treatment of systems with strong correlations. When, as in this work, we use operators coming from the hierarchy of the equations of motion as basic fields,[27,28] the COM is similar to the SDA.[11,24–26] However, the COM gives the possibility of choosing the basic fields according to the physics of the system under investigation. This freedom allows a better control on the dynamical information still present in the generalized mean-field approximation. Let us emphasize that even in the pole approximation the electronic self-energy is not trivial as in the standard mean-field approach, but a pole expansion of the exact electronic self-energy is used. Another fundamental difference between the COM and the approaches mentioned above consists of a treatment of the higher-order correlation functions occurring in the energy matrix [Eq. (2.4)], which are not directly related to elements of the Green's function. As shown in a recent publication,[20] there is no freedom in choosing the equations to compute those parameters, as they have to be used to fix the representation according to the relation

$$\lim_{\substack{j\to i\\ t\to 0^+}} S(i,j,t)=\langle \Psi(i)\Psi^\dagger(i)\rangle, \tag{2.9}$$

where the left-hand side comes from Eq. (2.7) and the right-hand side derives from the basic algebraic properties of the electronic field algebra—namely, the *Pauli principle*. Any other choice of the self-consistent equations that fix those parameters will lead to a representation for the Green's function, where the main symmetries of the system are violated.[28] In the case of the Hubbard model, Eq. (2.9) leads to the self-consistent equations

$$\langle \xi_\sigma(i)\,\eta^\dagger_\sigma(i)\rangle=0, \tag{2.10a}$$

$$\langle \xi_\uparrow(i)\xi^\dagger_\uparrow(i)\rangle=\langle \xi_\downarrow(i)\xi^\dagger_\downarrow(i)\rangle. \tag{2.10b}$$

The use of these equations, in the paramagnetic phase, led to a good agreement of the COM with the numerical results for the local, integrated, and thermodynamic quantities.[15,22,23]

In contrast to the paramagnetic solution—characterized by a complete translational and spin rotational symmetry—where the number of parameters in the energy matrix emerging from higher-order correlation functions is equal to the number of constrains given by the Pauli principle [Eq. (2.10)], an antiferromagnetic solution with two composite fields, which is characterized by a broken translational and spin rotational symmetry (they are, however, not broken in a completely independent way), requires additional parameters to satisfy all constraints emerging from the algebraic properties of the basic field operators ξ and η. It turns out that for extensions of a simple Hubbard model [Eq. (2.1)] by a next-nearest-neighbor hopping term (the t-t'-U model), or by a nearest-neighbor Coulomb repulsion (the so-called extended Hubbard model), the number of those parameters is equal to the number of "algebraic" constraints in the case of an antiferromagnetic solution. According to this, in the following we will investigate the antiferromagnetic solution of the 2D and 3D t-t'-U model in the limit of t' going to zero, and that of the 2D extended Hubbard model. For the antiferromagnetic solution, the two poles corresponding to the two composite fields ξ and η will split up into four poles due to the broken translational and spin rotational symmetry.

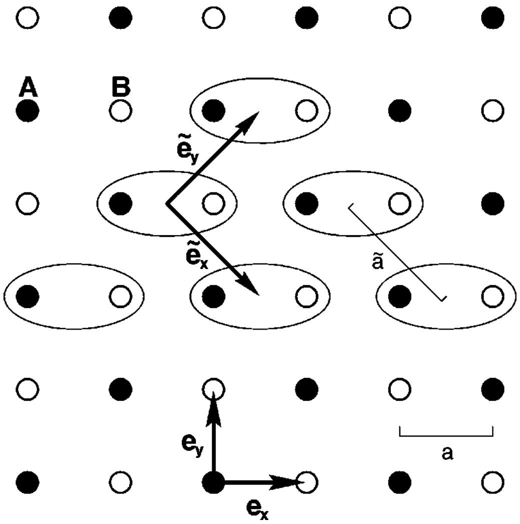

FIG. 1. The bipartite lattice structure induced by the antiferromagnetic ordering on a two-dimensional square lattice.

III. ANTIFERROMAGNETIC SOLUTION FOR THE HUBBARD MODEL

A. Antiferromagnetic solution on a bipartite lattice

As stated above, we will study the antiferromagnetic solution of the Hubbard model by considering the $t'\to 0$ limit of the t-t'-U model. The Hamiltonian of the latter reads

$$H^{tt'U}=\sum_{ij;\sigma}(t_{ij}+t'_{ij}-\mu\delta_{ij})c^\dagger_\sigma(i)c_\sigma(j)+U\sum_i n_\uparrow(i)n_\downarrow(i), \tag{3.1}$$

where the t'_{ij} matrix describes the next-nearest-neighbor hopping. The t' hopping is an intra-sublattice hopping for each of the two sublattices **A** and **B** of a bipartite square lattice, whereas the t hopping is an intersublattice hopping.

In this paper, we consider an antiferromagnetic solution of Hamiltonian (3.1), characterized by an opposite sign in the spin density on nearest-neighboring lattice sites. Thus the antiferromagnetic ordering induces a magnetic lattice $\{\tilde{\mathbf{R}}_i\}$ with a lattice constant $\tilde{a}=a\sqrt{2}$, overlying the chemical Bravais lattice $\{\mathbf{R}_i\}$ with lattice constant a. As shown in Fig. 1, the magnetic lattice is obtained as a square lattice with a basis, by collecting together two neighboring sites of the chemical lattice.

During the calculation of the Green's functions it will be convenient to switch between two equivalent representations of the system constructed on the chemical and magnetic lattices. We denote vectors belonging to the chemical lattice by their bare symbols, whereas the corresponding vectors on the magnetic lattice are denoted by an additional tilde. We impose the following global boundary conditions on the antiferromagnetic thermal equilibrium state.

Assumption III.1 The antiferromagnetic thermal equilibrium state has to satisfy the following global boundary conditions:

1. The particle and spin densities are globally conserved.

2. The mean value of the local particle density per spin satisfies the relation

$$\langle n_\sigma(i)\rangle = \tfrac{1}{2}[n-(-1)^\sigma m\cos(\mathbf{Q}\cdot\mathbf{R}_i)], \tag{3.2}$$

where m is the staggered magnetization, which has to be calculated self-consistently. The particle density n is imposed as an external parameter. Further we adopt the convention $\sigma=1,2$ for $\sigma=\uparrow,\downarrow$ and $\mathbf{Q}=(\pi/a,\pi/a)$.

3. All expectation values are invariant under the contemporary exchange of the spin direction and the sublattice index.

4. The normalization matrix I and the m matrix from Eqs. (2.5) and (2.6) have to be real.

We remark that conditions (1)–(3) are natural boundary conditions for an antiferromagnetic thermal equilibrium state characterized by a staggered magnetization, whereas condition (4) is a direct consequence of the fact that we are looking for a state without quasiparticle damping, as required by the approximation scheme described in Sec. II.

To reduce the computational effort in solving the integral self-consistent equations, we use a *spherical approximation* for the t' hopping, characterized by an additional hopping to next-next-nearest-neighbors with half the weight of the next-nearest-neighbor hopping, in the calculations of the integrals in the momentum space. This permits a definition of the t'-hopping matrix by $\alpha(\mathbf{k})$ only, and therefore reduces the number of evaluations to $O(N)$—N is the number of steps in the integrals—independently from the dimensionality of the system, while it would have been $O(N^d)$ for a d-dimensional system with the usual next-nearest-neighbor t'-hopping matrix. In two dimensions the t'-hopping matrix is given by $t'_{ij}=-12t'\beta_{ij}=-12t'(1/N)\Sigma_{\mathbf{k}}e^{i\mathbf{k}\cdot(\mathbf{R}_i-\mathbf{R}_j)}\beta(\mathbf{k})$ with $\beta(\mathbf{k})=\frac{1}{3}(4[\alpha(\mathbf{k})]^2-1)$. In three dimensions we find $t'_{ij}=-30t'\beta_{ij}=-30t'(1/N)\Sigma_{\mathbf{k}}e^{i\mathbf{k}\cdot(\mathbf{R}_i-\mathbf{R}_j)}\beta(\mathbf{k})$, with $\beta(\mathbf{k})=\frac{2}{5}(3[\alpha(\mathbf{k})]^2-\frac{1}{2})$. Let us remark that in the present definitions the hopping per lattice site is always normalized to 1. It is worth noting that, as we will take the $t'\to 0$ limit hereafter, the use of the *spherical approximation* cannot affect at all the results we will obtain.

In the following we will restrict our analysis to the 2D case. The 3D case, which might be treated in complete analogy by renormalizing the hopping constants and by changing the projections α_{ij} and β_{ij}, will be considered in Sec. IV C.

B. Normalization and energy matrices

In order to calculate the energy matrix in the two-pole approximation under the antiferromagnetic boundary conditions given in assumption III.1, we proceed along the guidelines given in Sec. II. To this end it is convenient to use the corresponding quantities defined on the chemical lattice, and to switch to the magnetic lattice only for the calculation of the Green's functions.

First, we calculate the full equation of motion for the composite field spinor [Eq. (2.2)] according to Eq. (2.3) for the t-t'-U Hamiltonian

$$i\frac{\partial}{\partial t}\Psi(i,t)=[\Psi(i,t),H^{tt'U}]=\begin{pmatrix} -\mu\xi_\uparrow(i,t)-4tc^\alpha_\uparrow(i,t)-4t\pi^\alpha_\uparrow(i,t)-12t'c^\beta_\uparrow(i,t)-12t'\pi^\beta_\uparrow(i,t)\\ -\mu\eta_\uparrow(i,t)+U\eta_\uparrow(i,t)+4t\pi^\alpha_\uparrow(i,t)+12t'\pi^\beta_\uparrow(i,t)\\ -\mu\xi_\downarrow(i,t)-4tc^\alpha_\downarrow(i,t)-4t\pi^\alpha_\downarrow(i,t)-12t'c^\beta_\downarrow(i,t)-12t'\pi^\beta_\downarrow(i,t)\\ -\mu\eta_\downarrow(i,t)+U\eta_\downarrow(i,t)+4t\pi^\alpha_\downarrow(i,t)+12t'\pi^\beta_\downarrow(i,t)\end{pmatrix}, \tag{3.3}$$

where we used the notation $\pi^\gamma_\sigma(i)=-n_{\bar\sigma}(i)c^\gamma_\sigma(i)+c^\dagger_{\bar\sigma}(i)c_\sigma(i)c^\gamma_{\bar\sigma}(i)+c_\sigma(i)c^{\gamma\dagger}_{\bar\sigma}(i)c_{\bar\sigma}(i)$ with $c^\gamma_\sigma(i)=\Sigma_j\gamma_{ij}c_\sigma(j)$, where $\gamma=\alpha,\beta$ stands for the projections defined in Sec. III A.

According to assumption III.1.1, the expectation values for spin-exchange operators vanish, and we find the general block structures

$$I=I_\uparrow\oplus I_\downarrow,\quad \varepsilon=\varepsilon_\uparrow\oplus\varepsilon_\downarrow,$$
$$M=M_\uparrow\oplus M_\downarrow,\quad S=S_\uparrow\oplus S_\downarrow. \tag{3.4}$$

The explicit form of the normalization matrix is obtained by direct evaluation of Eq. (2.5),

$$I(i,j)=\delta_{ij}I^{(n)}+\delta_{ij}I^{(m)}\cos(\mathbf{Q}\cdot\mathbf{R}_i), \tag{3.5}$$

with $I^{(n)}=\hat I^{(n)}\oplus\hat I^{(n)}$ and $I^{(m)}=\hat I^{(m)}\oplus-\hat I^{(m)}$, where the blocks are given by

$$\hat I^{(n)}=\begin{pmatrix}1-\dfrac{n}{2} & 0\\ 0 & \dfrac{n}{2}\end{pmatrix},\quad \hat I^{(m)}=\begin{pmatrix}\dfrac{m}{2} & 0\\ 0 & -\dfrac{m}{2}\end{pmatrix}. \tag{3.6}$$

For the m matrix, from Eq. (2.6) we obtain

$$m(i,j)=\delta_{ij}M_1+\alpha_{ij}M_3+\beta_{ij}M_5 +\cos(\mathbf{Q}\cdot\mathbf{R}_i)(\delta_{ij}M_2+\alpha_{ij}M_4+\beta_{ij}M_6). \tag{3.7}$$

The matrices $M_1,\dots,M_6$ also have the above-mentioned block structures

$$M_1=\begin{pmatrix}\hat{M}_1 & \mathbf{0}\\ \mathbf{0} & \hat{M}_1\end{pmatrix},\quad M_2=\begin{pmatrix}\hat{M}_2 & \mathbf{0}\\ \mathbf{0} & -\hat{M}_2\end{pmatrix},$$
$$M_3=\begin{pmatrix}\hat{M}_3 & \mathbf{0}\\ \mathbf{0} & \hat{M}_3\end{pmatrix},\quad M_4=\begin{pmatrix}\hat{M}_4 & \mathbf{0}\\ \mathbf{0} & -\hat{M}_4\end{pmatrix},\tag{3.8}$$
$$M_5=\begin{pmatrix}\hat{M}_5 & \mathbf{0}\\ \mathbf{0} & \hat{M}_5\end{pmatrix},\quad M_6=\begin{pmatrix}\hat{M}_6 & \mathbf{0}\\ \mathbf{0} & -\hat{M}_6\end{pmatrix},$$

with

$$\hat{M}_1=\begin{pmatrix}-\mu\left(1-\frac{1}{2}n\right)-4t(\Delta_\downarrow^\alpha+\Delta_\uparrow^\alpha)-6t'(\Delta_\downarrow^\beta+\Delta_\uparrow^\beta) & 4t(\Delta_\downarrow^\alpha+\Delta_\uparrow^\alpha)+6t'(\Delta_\downarrow^\beta+\Delta_\uparrow^\beta)\\ 4t(\Delta_\downarrow^\alpha+\Delta_\uparrow^\alpha)+6t'(\Delta_\downarrow^\beta+\Delta_\uparrow^\beta) & (U-\mu)\frac{1}{2}n-4t(\Delta_\downarrow^\alpha+\Delta_\uparrow^\alpha)-6t'(\Delta_\downarrow^\beta+\Delta_\uparrow^\beta)\end{pmatrix},$$

$$\hat{M}_2=\begin{pmatrix}-\mu\frac{m}{2}-4t(\Delta_\downarrow^\alpha-\Delta_\uparrow^\alpha)-6t'(\Delta_\downarrow^\beta-\Delta_\uparrow^\beta) & 4t(\Delta_\downarrow^\alpha-\Delta_\uparrow^\alpha)+6t'(\Delta_\downarrow^\beta-\Delta_\uparrow^\beta)\\ 4t(\Delta_\downarrow^\alpha-\Delta_\uparrow^\alpha)+6t'(\Delta_\downarrow^\beta-\Delta_\uparrow^\beta) & -\frac{m}{2}(-\mu+U)-4t(\Delta_\downarrow^\alpha-\Delta_\uparrow^\alpha)-6t'(\Delta_\downarrow^\beta-\Delta_\uparrow^\beta)\end{pmatrix},$$

$$\hat{M}_3=\begin{pmatrix}-4t(1-n+p) & -4t\left(\frac{1}{2}n-p\right)\\ -4t\left(\frac{1}{2}n-p\right) & -4tp\end{pmatrix},\quad \hat{M}_5=\begin{pmatrix}-12t'\left[1-n+\frac{1}{2}(p_\downarrow^\beta+p_\uparrow^\beta)\right] & -12t'\left[\frac{1}{2}n-\frac{1}{2}(p_\downarrow^\beta+p_\uparrow^\beta)\right]\\ -12t'\left[\frac{1}{2}n-\frac{1}{2}(p_\downarrow^\beta+p_\uparrow^\beta)\right] & -6t'(p_\downarrow^\beta+p_\uparrow^\beta),\end{pmatrix},\tag{3.9}$$

$$\hat{M}_4=\begin{pmatrix}0 & -2tm\\ 2tm & 0\end{pmatrix},\quad \hat{M}_6=\begin{pmatrix}-12t'\left[m+\frac{1}{2}(p_\downarrow^\beta-p_\uparrow^\beta)\right] & 6t'(m+p_\downarrow^\beta-p_\uparrow^\beta)\\ 6t'(m+p_\downarrow^\beta-p_\uparrow^\beta) & -6t'(p_\downarrow^\beta-p_\uparrow^\beta)\end{pmatrix}.$$

To shorten the notation of the occurring expectation values, we defined the following parameters:

$$\Delta_\sigma^\alpha=\frac{1}{2}(\langle\xi_\sigma(i)c_\sigma^{\alpha\dagger}(i)\rangle-\langle c_\sigma^\alpha(i)\,\eta_\sigma^\dagger(i)\rangle)\quad\text{for}\ \ i\in\mathbf{A}$$

$$p=\frac{1}{4}\langle n_\mu(i)n_\mu^\alpha(i)\rangle-\langle c_\uparrow(i)c_\downarrow(i)[c_\downarrow^\dagger(i)c_\uparrow^\dagger(i)]^\alpha\rangle,$$

$$\Delta_\sigma^\beta=\langle\xi_\sigma(i)c_\sigma^{\beta\dagger}(i)\rangle-\langle c_\sigma^\beta(i)\,\eta_\sigma^\dagger(i)\rangle\quad\text{for}\ \ i\in\mathbf{A},\tag{3.10}$$

$$p_\sigma^\beta=\frac{1}{4}\langle[n_1(i)-(-)^\sigma in_2(i)][n_1(i)+(-)^\sigma in_2(i)]^\beta\rangle$$
$$+\langle n_\sigma(i)n_\sigma^\beta(i)\rangle-\langle c_{\bar{\sigma}}(i)c_\sigma(i)[c_\sigma^\dagger(i)c_{\bar{\sigma}}^\dagger(i)]^\beta\rangle$$
$$\text{for}\ \ i\in\mathbf{A}.$$

Furthermore, we used the notation $n_\mu(i)=c^\dagger(i)\sigma_\mu c(i)$ for the spin- and charge-density operators with the Pauli spin matrices $\sigma_\mu\in\{\mathbf{1},\sigma_x,\sigma_y,\sigma_z\}$ and the electronic field spinors $c^\dagger(i)=[c_\uparrow^\dagger(i),c_\downarrow^\dagger(i)]$.

As the antiferromagnetic ordering breaks the translational invariance, the parameters Δ_σ^α, p, Δ_σ^β, and p_σ^β in principle do depend on the lattice site i. However, the antiferromagnetic state enjoys a translational invariance within each of the two sublattices **A** and **B**. For definitions of parameters (3.10) we arbitrarily chose the values on the sublattice **A**. Their values on the sublattice **B** are then given by exchanging the spin indices according to assumption III.1.3.

The operators, from which the expectation values for the parameters Δ_σ^α, p, Δ_σ^β, and p_σ^β are taken, are not Hermitian. However, the corresponding parameters have to be real according to assumption III.1.4. This finally results in the parameter p being independent of both the spin and the sublattice. Furthermore, the normalization matrix and the m-matrix result to be symmetric.

To calculate the energy matrix we note that Eq. (2.4) gives $m=\varepsilon I$. In Fourier space, we have

$$
\begin{aligned}
m(\mathbf{k},\mathbf{p}) &= \frac{a^2}{(2\pi)^2}\int_{\Omega_B} \mathrm{d}^2 q\ \varepsilon(\mathbf{k}+\mathbf{q},\mathbf{p}-\mathbf{q}) I(\mathbf{q}) \\
&= \varepsilon(\mathbf{k},\mathbf{p}) I^{(n)} + \varepsilon(\mathbf{k}+\mathbf{Q},\mathbf{p}-\mathbf{Q}) I^{(m)},
\end{aligned} \tag{3.11}
$$

where the Fourier transform of the normalization and the m matrix are given by

$$
I(\mathbf{k},\mathbf{p}) = \left(\frac{2\pi}{a}\right)^2 [\delta(\mathbf{p}) I^{(n)} + \delta(\mathbf{p}-\mathbf{Q}) I^{(m)}]
$$

$$
\begin{aligned}
m(\mathbf{k},\mathbf{p}) = \left(\frac{2\pi}{a}\right)^2 \{ & \delta(\mathbf{p})[M_1 + \alpha(\mathbf{k}) M_3 + \beta(\mathbf{k}) M_5] \\
& + \delta(\mathbf{p}-\mathbf{Q})[M_2 + \alpha(\mathbf{k}) M_4 + \beta(\mathbf{k}) M_6]\}.
\end{aligned} \tag{3.12}
$$

We recall that the Fourier transform on the chemical lattice is defined as in Eq. (2.7) to benefit from the periodicity of the thermal equilibrium states.

Using the $2\mathbf{Q}$ periodicity of the thermal equilibrium states in Eq. (3.11), we obtain the energy matrix in Fourier space,

$$
\varepsilon(\mathbf{k},\mathbf{p}) = m(\mathbf{k},\mathbf{p}) C - m(\mathbf{k}+\mathbf{Q},\mathbf{p}-\mathbf{Q}) D, \tag{3.13}
$$

with

$$
\begin{aligned}
C &= (I^{(m)})^{-1}[I^{(n)}(I^{(m)})^{-1} - I^{(m)}(I^{(n)})^{-1}]^{-1}, \\
D &= (I^{(n)})^{-1}[I^{(n)}(I^{(m)})^{-1} - I^{(m)}(I^{(nt)})^{-1}]^{-1}.
\end{aligned} \tag{3.14}
$$

Using the explicit expressions 3.12 for m and the normalization matrix, we can write the energy matrix as

$$
\begin{aligned}
\varepsilon(\mathbf{k},\mathbf{p}) = \left(\frac{2\pi}{a}\right)^2 \{ & \delta(\mathbf{p})[\varepsilon^{(1)} + \alpha(\mathbf{k})\varepsilon^{(2)} + \beta(\mathbf{k})\varepsilon^{(5)}] \\
& + \delta(\mathbf{p}-\mathbf{Q})[\varepsilon^{(3)} + \alpha(\mathbf{k})\varepsilon^{(4)} + \beta(\mathbf{k})\varepsilon^{(6)}]\},
\end{aligned} \tag{3.15}
$$

with

$$
\begin{aligned}
\varepsilon^{(1)} &= M_1 C - M_2 D, \quad \varepsilon^{(2)} = M_3 C + M_4 D, \\
\varepsilon^{(3)} &= M_2 C - M_1 D, \quad \varepsilon^{(4)} = M_4 C + M_3 D, \\
\varepsilon^{(5)} &= M_5 C - M_6 D, \quad \varepsilon^{(6)} = M_6 C - M_5 D.
\end{aligned} \tag{3.16}
$$

C. Green's functions

The solutions of the linearized equation of motion (2.8) with expression (3.15) for the energy matrix can be interpreted as translational invariant Green's functions $S^{AA}(\tilde{\mathbf{k}},\omega)$, $S^{AB}(\tilde{\mathbf{k}},\omega)$, $S^{BA}(\tilde{\mathbf{k}},\omega)$, and $S^{BB}(\tilde{\mathbf{k}},\omega)$ on the magnetic lattice, as shown in Appendix A. They have the general structure

$$
\begin{aligned}
S^{XY}(\tilde{\mathbf{k}},\omega) = & [\omega^2 + \omega A^{XY}(\tilde{\mathbf{k}}) + B^{XY}(\tilde{\mathbf{k}})]^{-1} \\
& \times [\omega C^{XY}(\tilde{\mathbf{k}}) + D^{XY}(\tilde{\mathbf{k}})].
\end{aligned} \tag{3.17}
$$

The explicit form of the coefficients A^{XY}, B^{XY}, C^{XY}, and D^{XY} are given in Appendix B.

Due to assumption III.1 on the antiferromagnetic thermal equilibrium state, Green's function (3.17) has the block structure $S^{XY} = S^{XY}_{\uparrow} \oplus S^{XY}_{\downarrow}$ shown in Eq. (3.4), where the poles $\{E^{XY}_{\sigma,i}(\tilde{\mathbf{k}}) | i \in \{1,2,3,4\}\}$ of the spin-dependent parts S^{XY}_{σ} of the Green's functions are given by the roots of the fourth-order equations

$$
\det[\omega^2 + \omega A^{XY}_{\sigma}(\tilde{\mathbf{k}}) + B^{XY}_{\sigma}(\tilde{\mathbf{k}})] = 0. \tag{3.18}
$$

The set of poles for the Green's functions S^{XY}_{σ} are all equal, i.e., the quasiparticle energies depend on neither the spin nor the sublattice. This reflects the property of the antiferromagnetic state with staggered magnetization, where the majority-spin states and the minority-spin states energetically occupy exactly the same regions and differ only in their corresponding spectral weights (cf. also Sec. IV). Therefore, we simply write $E_i(\tilde{\mathbf{k}}) = E^{XY}_{\sigma,i}(\tilde{\mathbf{k}})$.

We can write the retarded Green's function (3.17) as

$$
S^{XY}_{\sigma}(\tilde{\mathbf{k}},\omega) = \lim_{\eta\to 0} \sum_{i=1}^{4} \frac{1}{\omega - E_i(\tilde{\mathbf{k}}) + i\eta} \sigma^{XY}_{\sigma,i}(\tilde{\mathbf{k}}), \tag{3.19}
$$

with $X,Y \in \{\mathbf{A},\mathbf{B}\}$, $\sigma \in \{\uparrow,\downarrow\}$ and the spin- and sublattice-dependent spectral weights $\sigma^{XY}_{\sigma,i}$ given by

$$
\begin{aligned}
\sigma^{XY}_{\sigma,i}(\tilde{\mathbf{k}}) = \frac{1}{\prod_{\substack{j=1\\ j\neq i}}^{4} [E_i(\tilde{\mathbf{k}}) - E_j(\tilde{\mathbf{k}})]} & \{[E_i(\tilde{\mathbf{k}})]^3 C^{XY}_{\sigma}(\tilde{\mathbf{k}}) + [E_i(\tilde{\mathbf{k}})]^2 \\
& \times \{D^{XY}_{\sigma}(\tilde{\mathbf{k}}) + \det[A^{XY}_{\sigma}(\tilde{\mathbf{k}})][A^{XY}_{\sigma}(\tilde{\mathbf{k}})]^{-1} C^{XY}_{\sigma}(\tilde{\mathbf{k}})\} \\
& + E_i(\tilde{\mathbf{k}})\{\det[A^{XY}_{\sigma}(\tilde{\mathbf{k}})][A^{XY}_{\sigma}(\tilde{\mathbf{k}})]^{-1} D^{XY}_{\sigma}(\tilde{\mathbf{k}})\} \\
& + \det[B^{XY}_{\sigma}(\tilde{\mathbf{k}})][B^{XY}_{\sigma}(\tilde{\mathbf{k}})]^{-1} C^{XY}_{\sigma}(\tilde{\mathbf{k}}) \\
& + \det[B^{XY}_{\sigma}(\tilde{\mathbf{k}})][B^{XY}_{\sigma}(\tilde{\mathbf{k}})]^{-1} D^{XY}_{\sigma}(\tilde{\mathbf{k}})\}.
\end{aligned} \tag{3.20}
$$

D. Self-consistency equations

Given the temperature T and the particle density n as external thermodynamic parameters, as well as the Coulomb interaction U and the hopping constants t and t', which are the model-dependent parameters, we are now able to give a closed set of self-consistent conditions for the internal parameters characterizing an antiferromagnetic thermal equilibrium state. These internal parameters are p, $p^{\beta}_{\uparrow}$, $p^{\beta}_{\downarrow}$, $\Delta^{\alpha}_{\uparrow}$, $\Delta^{\alpha}_{\downarrow}$, $\Delta^{\beta}_{\uparrow}$, and $\Delta^{\beta}_{\downarrow}$ from Eq. (3.10), the chemical potential μ, and the magnetization m from Eq. (3.2).

For the calculations of these parameters we need a knowledge of the correlation functions, which are connected to the retarded Green's functions of the fundamental spinor by means of the spectral theorem. In view of the special form [Eq. (3.19)] of the retarded Green's functions, the spectral theorem at equal time may be written as

$$C^{XY}(\tilde{\mathbf{R}}_i,\tilde{\mathbf{R}}_j)=\langle\Psi^X(\tilde{\mathbf{R}}_i)\Psi^{Y\dagger}(\tilde{\mathbf{R}}_j)\rangle$$
$$=\frac{1}{2}\,\frac{\tilde{a}^2}{(2\pi)^2}\sum_{l=1}^{4}\int_{\Omega_{\tilde{B}}}d^2\tilde{k}\;e^{i\tilde{\mathbf{k}}\cdot(\tilde{\mathbf{R}}_i-\tilde{\mathbf{R}}_j)}\sigma_l^{XY}(\tilde{\mathbf{k}})$$
$$\times\left[1+\tanh\left(\frac{E_l(\tilde{\mathbf{k}})}{2k_BT}\right)\right].\qquad(3.21)$$

We denote the on-site, nearest-neighbor, and next-(next)-nearest-neighbor correlation functions at equal time by $C^{XX}(\tilde{\mathbf{R}}_i)$, $C^{XY\tilde{\alpha}}(\tilde{\mathbf{R}}_i)$, and $C^{XX\tilde{\beta}}(\tilde{\mathbf{R}}_i)$.

For the parameters μ and m, we then find the self-consistent equations

$$2-n=C_{11}^{AA}(\tilde{\mathbf{R}}_i)+C_{11}^{BB}(\tilde{\mathbf{R}}_i)+C_{22}^{AA}(\tilde{\mathbf{R}}_i)+C_{22}^{BB}(\tilde{\mathbf{R}}_i),$$
$$2m=C_{44}^{AA}(\tilde{\mathbf{R}}_i)-C_{22}^{AA}(\tilde{\mathbf{R}}_i)+C_{22}^{BB}(\tilde{\mathbf{R}}_i)-C_{44}^{BB}(\tilde{\mathbf{R}}_i)].\qquad(3.22a)$$

The parameters $\Delta_\uparrow^\alpha$, $\Delta_\downarrow^\alpha$, $\Delta_\uparrow^\beta$, and $\Delta_\downarrow^\beta$ are directly related to matrix elements of the correlation functions by

$$\Delta_\uparrow^\alpha=\tfrac{1}{2}[C_{11}^{AB\tilde{\alpha}}(\tilde{\mathbf{R}}_i)+C_{12}^{AB\tilde{\alpha}}(\tilde{\mathbf{R}}_i)-C_{12}^{BA\tilde{\alpha}}(\tilde{\mathbf{R}}_i)-C_{22}^{BA\tilde{\alpha}}(\tilde{\mathbf{R}}_i)],$$
$$\Delta_\downarrow^\alpha=\tfrac{1}{2}[C_{33}^{AB\tilde{\alpha}}(\tilde{\mathbf{R}}_i)+C_{34}^{AB\tilde{\alpha}}(\tilde{\mathbf{R}}_i)-C_{34}^{BA\tilde{\alpha}}(\tilde{\mathbf{R}}_i)-C_{44}^{BA\tilde{\alpha}}(\tilde{\mathbf{R}}_i)],\qquad(3.22b)$$

$$\Delta_\uparrow^\beta=[C_{11}^{AA\tilde{\beta}}(\tilde{\mathbf{R}}_i)-C_{22}^{AA\tilde{\beta}}(\tilde{\mathbf{R}}_i)],$$
$$\Delta_\downarrow^\beta=[C_{11}^{BB\tilde{\beta}}(\tilde{\mathbf{R}}_i)-C_{22}^{BB\tilde{\beta}}(\tilde{\mathbf{R}}_i)].$$

The parameters p, $p_\uparrow^\beta$, and $p_\downarrow^\beta$ cannot be calculated explicitly by the single-particle Green's function [Eq. (3.19)], because they derive from higher-order correlation functions. According to what was stated in Sec. II, we will use the following equations to fix the representation of the Green's function:[15,21]

$$C_{12}^{AA}(\tilde{\mathbf{R}}_i)=0,$$
$$C_{12}^{BB}(\tilde{\mathbf{R}}_i)=0,\qquad(3.22c)$$
$$C_{11}^{AA}(\tilde{\mathbf{R}}_i)=C_{33}^{AA}(\tilde{\mathbf{R}}_i).$$

We observe that all self-consistent equations are coupled, and have to be solved as one set by means of a global convergency scheme.

Finally we remark that the correlation functions $C^{XX}(\tilde{\mathbf{R}}_i)$, $C^{XY\tilde{\alpha}}(\tilde{\mathbf{R}}_i)$, and $C^{XX\tilde{\beta}}(\tilde{\mathbf{R}}_i)$ actually do not depend on the lattice site $\mathbf{R}_i$ of the magnetic lattice because of the translational invariance enjoyed by the Green's functions [Eq. (3.19)].

IV. NUMERICAL EVALUATION OF THE ANTIFERROMAGNETIC PHASE FOR THE HUBBARD MODEL

In the following the thermodynamics of the antiferromagnetic thermal equilibrium states for the Hubbard model in two and three dimensions is discussed. We report the phase diagrams resulting from solutions of Eqs. (3.22), as well as some of the microscopic properties of the corresponding solutions, which explain the phase behavior. In this context, our main concern is in the interplay of the antiferromagnetic (Mott-Heisenberg) gap and the Mott-Hubbard gap leading to a metal-insulator transition in the antiferromagnetic phase. Furthermore, we investigate the distribution of the spectral weight between the majority- and minority-spin states that explains most of the phase properties found for the antiferromagnetic solution. As a first step, we establish an averaging procedure between solutions for positive and negative values of t' that is capable of ruling out a nonphysical artifact induced by the spherical approximation, and of establishing the correspondence to the simple Hubbard model.

A. Averaging procedure in t'

Due to the incompatibility of the nearest- and the next-nearest-neighbor hoppings the t-t'-U model does not enjoy particle-hole symmetry at half-filling $(n=1)$. In addition, the spherical approximation for the t' hopping overemphasizes the intrasublattice hopping to the next- and next-next-nearest neighbors. This leads to an instability of the antiferromagnetic solution for the t-t'-U model at half-filling: the magnetization goes to zero for positive values of the t' hopping, and for negative values of t' diverges to infinity [cf. Fig. 2(a)]. Positive values of the intrasublattice hopping do suppress antiferromagnetism to a certain extent, whereas negative values are in favor of it by the additional phase factor of π.

For a simple Hubbard model the particle-hole symmetry reflects the algebraic property

$$\mu(n=1)=\frac{U}{2}.\qquad(4.1a)$$

For an antiferromagnetic solution in the framework of the two-pole approximation, we have the additional condition

$$\Delta_\uparrow^\alpha(n=1)=-\Delta_\downarrow^\alpha(n=1),\qquad(4.1b)$$

which is a generalization of the condition $\Delta_\uparrow^\alpha(n=1)=0=\Delta_\downarrow^\alpha(n=1)$, imposed by the particle-hole symmetry on the paramagnetic solution of the simple Hubbard model, because of the inequivalence of the majority and the minority spin subsystems in the antiferromagnetic state. Condition (4.1a) is satisfied in the limit t' going to zero independently of the direction [see Fig. 2(b)]. This is a direct consequence of the fact that the proper representation for the Green's functions has been taken by using the complete set[20,28] of constraints coming from the Pauli principle [Eq. (3.22c)].

Taking the average between the solutions for t' and $-t'$ with $|t'|$ approaching zero, we obtain an antiferromagnetic state—which formally has zero t' hopping—that satisfies Eqs. (4.1), has no divergence in the magnetization and the other parameters at half filling [see Figs. 2(a), 2(c), and 2(d)] and can be considered as representative of the simple Hubbard model. Averaging the solutions for $\pm t'$ thus combines the large benefit in computational time provided by the

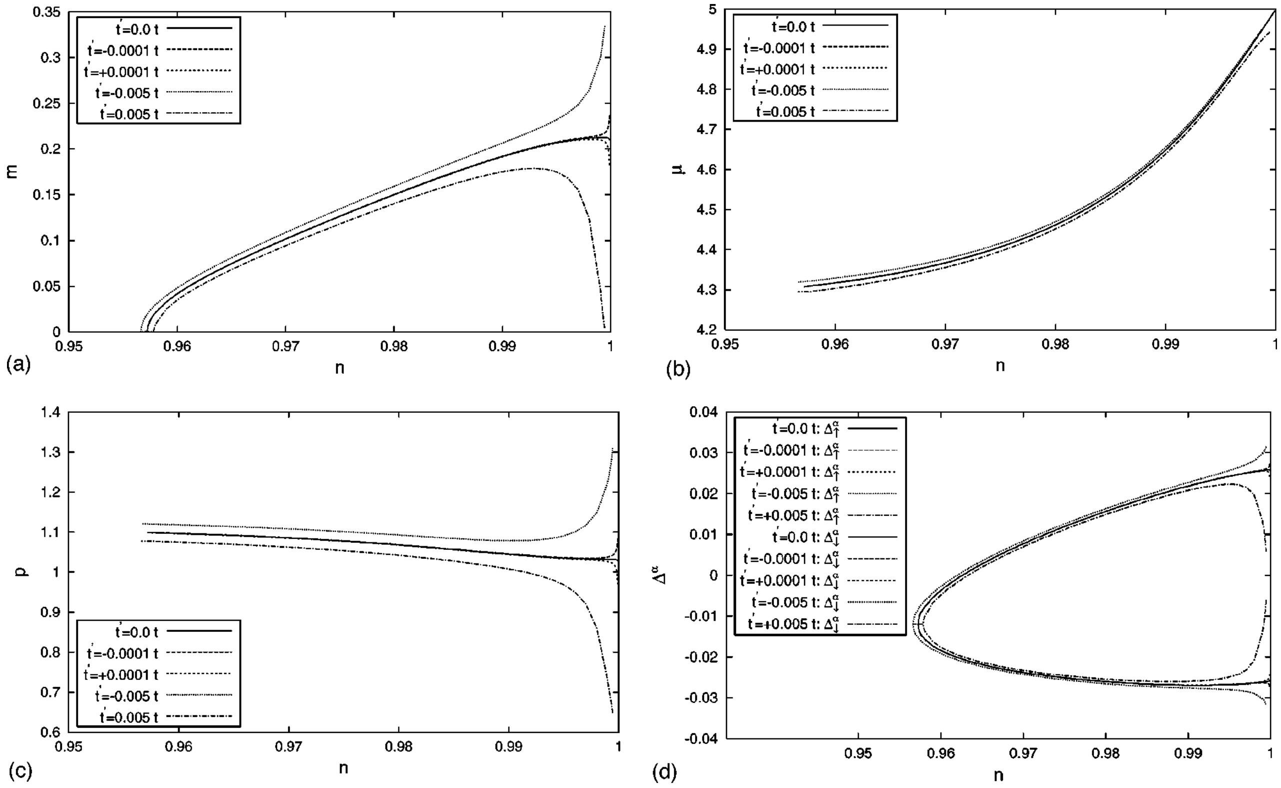

FIG. 2. The average algorithm between positive and negative values of t' in the 2D t-t'-U model for $U=10t$ and $kT=0.5t$. (a) Sublattice magnetization as a function of n. (b) Chemical potentials as a function of n. (c) The parameter p as a function of n. (d) The parameters Δ^{α} as a function of n.

spherical approximation with an antiferromagnetic solution that satisfies the complete set of symmetry constrains deriving from the Pauli principle and enjoys the particle-hole symmetry. The numerically accessible limit for the t' hopping, which has been used in combination with the above averaging procedure (see Fig. 2), is $t'=\pm 10^{-4}t$. Hereafter, we will present results exclusively from the averaged solution, and we will consider them as results of the simple Hubbard model.

B. The antiferromagnetic state of the Hubbard model

1. Phase diagram

The n-T and U-n phase diagrams for the antiferromagnetic state of the 2D Hubbard model and the corresponding paramagnetic state are shown in Figs. 3 and 4. The antiferromagnetic state has a free energy lower than the one of the paramagnetic state over the whole phase region, leading to a phase transition of second order between the antiferromag-

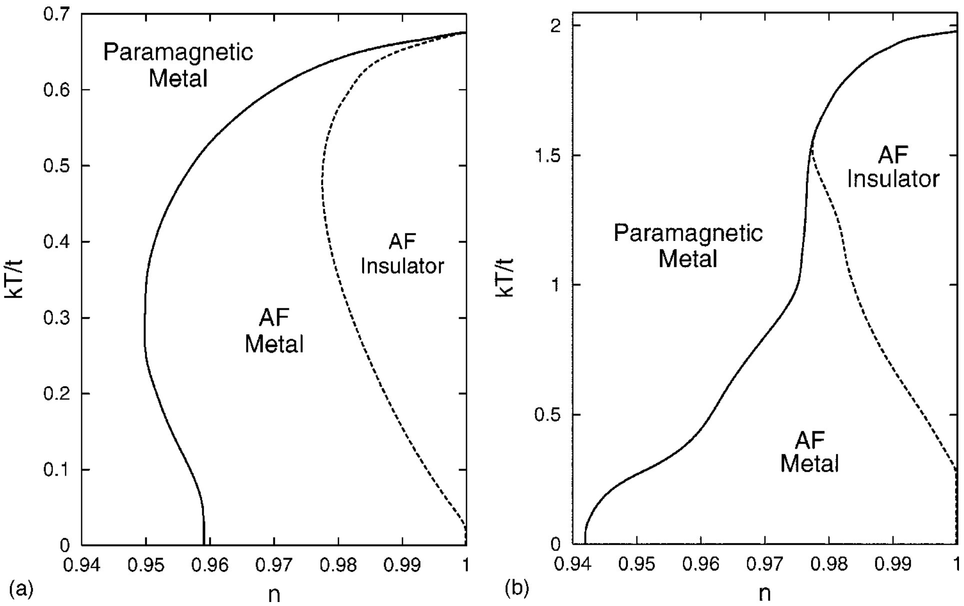

FIG. 3. The n-T phase diagram for the 2D Hubbard model. (a) $U=10t$. (b) $U=20t$.

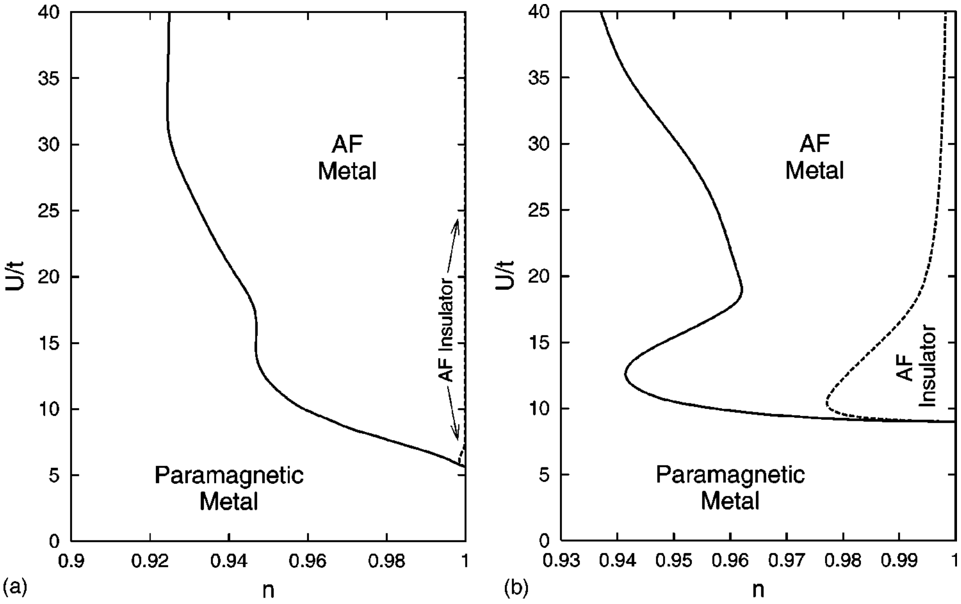

FIG. 4. The U-n phase diagram for the 2D Hubbard model. (a) $kT=0.01t$. (b) $kT=0.5$.

netic and paramagnetic phases at the lines of vanishing magnetization. The study of the phase diagram near half-filling has to be completed by an investigation of the ferromagnetic phase[30] and the charge-ordered phase, which both can be studied in the framework of the approximation scheme described above. The antiferromagnetic phase could be energetically ruled out by one of these other phases in certain regions of the phase diagrams, thus leading to phase transitions of first order.[26,31–33] In this section we give a brief overview of the properties of the antiferromagnetic phase, which then will be related to the inner structure of the antiferromagnetic state—namely its density of states—in the subsequent sections.

The most striking features of the antiferromagnetic phase are the finite critical Coulomb interaction U_c as a lower bound to the antiferromagnetic state at half-filling, the restriction of the antiferromagnetic state to a very narrow region in n around half-filling, and the metal-insulator transition (MIT) within the antiferromagnetic phase. The vanishing of the staggered magnetization at half filling for $U<U_c$—we find U_c within $5t$–$10t$ (see Fig. 4)—is supposed to be an effect of strong electron correlations. It cannot be observed within simple mean-field treatments of the Hubbard model,[34–36] where the antiferromagnetic phase is stable down to $U=0$ at $n=1$. Also, in more sophisticated mean-field approximations, such as the SDA, a stable antiferromagnetic state is found at $n=1$ down to very small values of U, and its stability down to $U=0$ cannot be excluded.[26] The same holds for the antiferromagnetic state of the simple Hubbard model treated by the DMFT.[37]

As we already mentioned in Sec. I, the SDA is rather closely related to the COM, but to calculate the antiferromagnetic state further approximations on the correlation functions are needed.[25,26] The main difference lies in the treatment of the internal parameters emerging from higher-order correlation functions. While the COM uses these to fix the representation of the Green's functions [Eq. (3.22c)], they are calculated by the equations of motion in the SDA.

In a previous study[38] we investigated the critical Coulomb interaction as a function of the t' hopping, showing that a finite value of U_c in the above-mentioned range has also to be expected in the exact limit $t'\rightarrow 0$.

The antiferromagnetic phase found in the high-T_c copper oxide compounds generally shows a great stability at half-filling, just a few percent of electron or hole doping leads to a strong reduction of the Néel temperature and eventually to the vanishing of the antiferromagnetic phase. On the other hand, it is well known that in general the mean-field treatment of the Hubbard model strongly overemphasizes the stability of the antiferromagnetic phase in doping. In the COM, where the strong correlation effects are restored to some extent by the Pauli principle symmetry constraint, the stability of the antiferromagnetic phase is actually reduced to a narrow region of a few percent of doping around half-filling with a strong reduction of the Néel temperature. For the Hubbard model such a behavior has been confirmed by numerical results in quantum Monte Carlo studies.[29,39] In contrast, a larger region for the antiferromagnetic phase has been obtained by the SDA (Ref. 26) and the $d=\infty$ approximation.[9,37]

At zero temperature a transition from an antiferromagnetic insulator at half-filling and an antiferromagnetic metal for $n<1$ is observed. At higher temperatures, however, we find an extended region in doping around $n=1$, where the Fermi level is situated inside the Mott-Heisenberg gap, which itself is large with respect to the thermal energy kT. We thus have a state with poor conductivity of semiconductor type, which we call an ''antiferromagnetic insulator.'' The metallic behavior is recovered when the Fermi level joins the second antiferromagnetic band with decreasing values of n.

The n-T phase diagrams show a strong qualitative difference in the low-temperature region according to the presence [Fig. 3(b)] or absence [Fig. 3(a)] of a Mott-Hubbard gap. For values of U that do not admit a Mott-Hubbard gap, the stability of the antiferromagnetic phase is enhanced by increasing temperature (a phenomenon called ''heat magnetization''), whereas the reverse is true for values of U where the Mott-Hubbard gap is already opened.

Furthermore, the presence of the Mott-Hubbard gap and the fact that it closes within the antiferromagnetic phase, when the particle density is reduced, is also responsible for the intermediate reduction of the stability of the antiferromagnetic state by increasing the Coulomb interaction (Fig. 4). This reduction is reinforced by increasing temperature and leads to a ''noselike'' shape of the U-n phase diagram. Both phenomena can be explained by the evolution of the spectral weights for the majority- and minority-spin subsystems as functions of the external parameters, as will be explained in detail in Sec. IV B 2.

Finally, we remark that the phase diagrams shown in Figs. 3 and 4 are completely symmetric with respect to $n=1$; this is due to the fact that the thermal equilibrium state respects the particle-hole symmetry. To incorporate the experimentally observed asymmetry in particle and hole doping, a projection of the two-band Hubbard model on an effective single-band one has been proposed.[33]

2. Band properties

The spectral properties of the antiferromagnetic state are deduced from the electronic single-particle Green's function on each sublattice $S^{XX}_{cc^\dagger}(\tilde{\mathbf{k}},\omega)$ with $X\in\{\mathbf{A},\mathbf{B}\}$. In the following we will restrict our analysis to the sublattice **A**, while the quantities on the sublattice **B** are obtained by simply exchanging the majority- and minority-spin subsystems. We thus have for the retarded electronic Green's function on the sublattice **A**:

$$S^{AA}_{cc^\dagger}(\tilde{\mathbf{k}},\omega)=S^{AA}_{\xi\xi^\dagger}(\tilde{\mathbf{k}},\omega)+S^{AA}_{\xi\eta^\dagger}(\tilde{\mathbf{k}},\omega)+S^{AA}_{\eta\xi^\dagger}(\tilde{\mathbf{k}},\omega)+S^{AA}_{\eta\eta^\dagger}(\tilde{\mathbf{k}},\omega). \tag{4.2}$$

The spin-dependent electronic density of states within the antiferromagnetic state is then given by

$$\begin{aligned}N^A_\sigma(\omega)&:=\left(\frac{\tilde{a}}{2\pi}\right)^2\int_{\Omega_{\tilde{B}}}d^2\tilde{k}\left(-\frac{1}{\pi}\,\mathrm{Im}\,S^{AA}_{cc^\dagger}(\tilde{\mathbf{k}},\omega)\right)\\&=\left(\frac{\tilde{a}}{2\pi}\right)^2\int_{\Omega_{\tilde{B}}}d^2\tilde{k}\sum_{i=1}^{4}\delta[\omega-E_i(\tilde{\mathbf{k}})][\sigma^{AA}_{i,\xi_\sigma\xi^\dagger_\sigma}(\tilde{\mathbf{k}},\omega)\\&\quad+\sigma^{AA}_{i,\xi_\sigma\eta^\dagger_\sigma}(\tilde{\mathbf{k}},\omega)+\sigma^{AA}_{i,\eta_\sigma\xi^\dagger_\sigma}(\tilde{\mathbf{k}},\omega)+\sigma^{AA}_{i,\eta_\sigma\eta^\dagger_\sigma}(\tilde{\mathbf{k}},\omega)].\end{aligned} \tag{4.3}$$

We recall that all energies refer to the chemical potential.

The two-pole approximation leads to a splitting of the single electronic band into two Hubbard subbands that correspond to the elementary excitations described by the composite operators ξ and η. Those two subbands are separated by the on-site Coulomb interaction U, which may lead to a gap at same critical value.[9,40] The bipartite lattice approach leads to a doubling of the two subbands by reflection around the band center at $(U/2)-\mu$ [see Fig. 6(c)]. In the paramagnetic case, when the magnetic lattice is introduced, this doubling of the Hubbard subbands by the reduction of the Brillouin zone is completely artificial: the reflected bands occupy exactly the same energy interval, with the same spectral weights as the original Hubbard subbands.

The antiferromagnetic state, however, is characterized by the opening of Mott-Heisenberg gaps at the crossing points of the four subbands induced by the switching to the magnetic lattice. Thus we find three Mott-Heisenberg gaps: one in the lower Hubbard band, (Δ_ξ), one in the upper Hubbard band, (Δ_η), and a central Mott-Heisenberg gap, $(\Delta_{\xi-\eta})$, in the region where the two Hubbard subbands overlap in the paramagnetic phase (see Fig. 5).

If the two Hubbard subbands are already separated by a Mott-Hubbard gap (in the paramagnetic phase it has been found[40] that the Mott-Hubbard gap opens at $U\simeq 13.2t$), the central Mott-Heisenberg gap adds to this gap [see Fig. 6(a)]. The gaps Δ_ξ and Δ_η are not symmetric around the Mott separation $\pm U/2$, because the upper and the lower band edges are shifted by different amounts.

The antiferromagnetic ordering thus leads to a splitting of the two Hubbard subbands into four antiferromagnetic bands that are occupied by both majority- and minority-spin subsystems. As can be seen from Fig. 5, the two spin subsystems energetically occupy the same regions—which is the reason why the staggered magnetization never reaches saturation $(m=n)$—but with rather different spectral weights: the spectral weight of the majority spins is strongly enhanced at the upper band edges, whereas the minority spins have an enhanced spectral weight at the lower band edges, leading to staggered magnetization. At half-filling the density of states shows a complete symmetry between the minority and majority spins with respect to reflection of the energy around the Fermi level. This is due to the fact that our solution respects the particle-hole symmetry.

(a) The Mott-Heisenberg and the Mott-Hubbard gap. The interplay between the Mott-Hubbard gap and the Mott-Heisenberg gap at half-filling is illustrated in Fig. 6. For $U=10t$ the two Hubbard subbands overlap at the Néel temperature T_{N}, and by decreasing T we find the opening of the Mott-Heisenberg gaps in the two Hubbard subbands as well as in the central region [Fig. 6(b)]. The corresponding

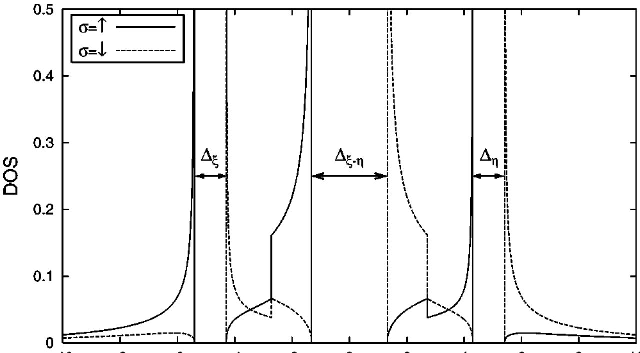

FIG. 5. The density of states on the sublattice **A**, illustrating the Mott-Heisenberg gaps in the lower and upper Hubbard bands, as well as in their overlapping region in the paramagnetic phase. The values of the parameters are $U=10t$, $n=1.0$, and $kT=0.01t$.

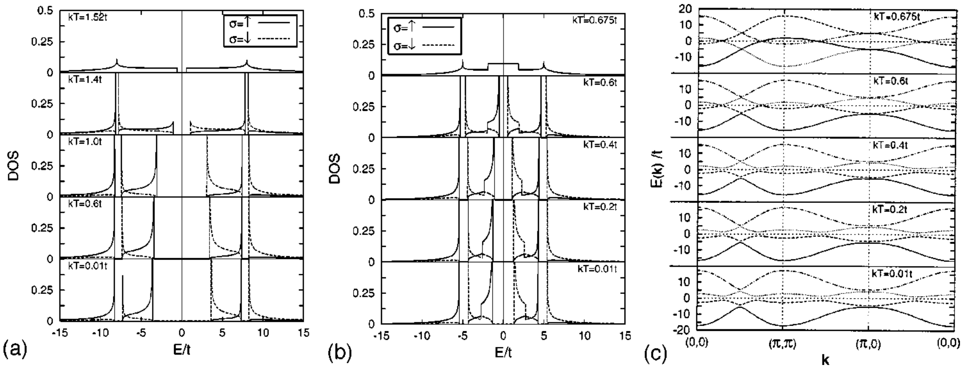

FIG. 6. Density of states and band structure at half-filling; the thin vertical line at $E=0$ denotes the position of the Fermi level E_F. (a) Sublattice density of states for $U=16$. (b) Sublattice density of states for $U=10t$. (c) Band structure on the chemical lattice for $U=10t$.

evolution of the electronic band structure in the Brillouin zone of the chemical lattice is shown in Fig. 6(c). We note the doubling of the Hubbard subbands in the paramagnetic state, which then evolves into the four antiferromagnetic subbands by decreasing temperature, and the typical symmetry of the band structure along the diagonal of the Brillouin zone for the chemical lattice due to the reduced Brillouin zone of the magnetic lattice.

In Fig. 6(a) the case for $U=16t$ is shown, where the Mott-Hubbard gap already separates the two Hubbard subbands in the paramagnetic phase just above the transition point. By decreasing temperature the Mott-Heisenberg gaps Δ_ξ and Δ_η open within each of the two Hubbard subbands. In addition, the central Mott-Heisenberg gap adds to the Mott-Hubbard gap, leading to the central gap $\Delta_{\xi-\eta}$.

The temperature dependence of these gaps is illustrated in Figs. 7(a) and 7(b) for various values of U. Above a certain critical value of U the central gap remains open at the phase transition. At low temperatures the Mott-Heisenberg gaps within the two Hubbard subbands, Δ_ξ and Δ_η, increase as a function of U up to a maximum value $U\approx 11t$, and then decrease like $1/U$ [cf. Fig. 7(c)]. This reflects the $1/U$ dependence of the antiferromagnetic exchange integral in the Heisenberg model, to which the half-filled Hubbard model can be mapped.[41,42] For the central gap the additional Mott separation prevents this behavior. Also, the Néel temperature does not show a $1/U$-like behavior (cf. Fig. 8), which indicates that the antiferromagnetic exchange integral is not always properly taken into account.

(b) The metal-insulator transition: The phenomenon of metal-insulator transitions has been intensively studied in the context of strongly correlated electron systems.[43] In the framework of the COM the MIT within the paramagnetic state at half-filling is found[40] in light of the Hubbard picture, due to a separation of the two Hubbard subbands at a critical value of the Coulomb interaction. This picture is quite different from the one found by the DMFT, where the MIT from a paramagnetic metal to a paramagnetic insulator is

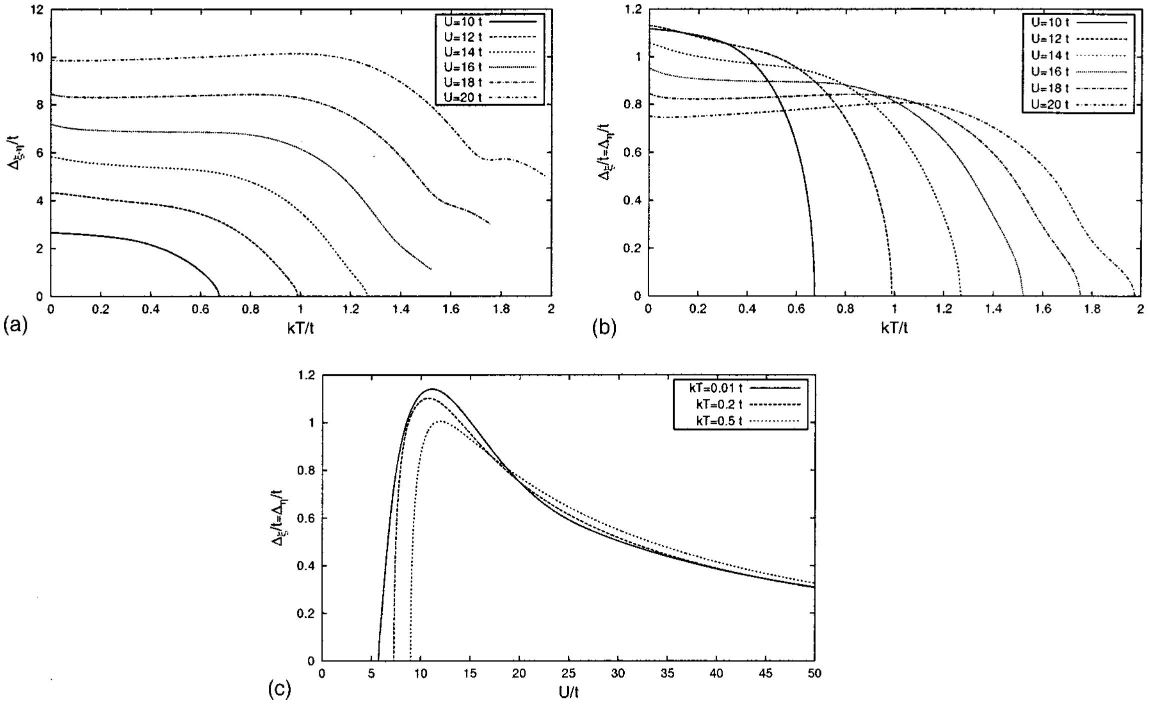

FIG. 7. The Mott gap and the Mott-Heisenberg gap at $n=1$. (a) Central gap $\Delta_{\xi-\eta}$ as function of T. (b) Gaps in the lower and the upper Hubbard band, Δ_ξ and Δ_η, as funciton of T. (c) Gaps in the lower and the upper Hubbard band, Δ_ξ and Δ_η, as function of U.

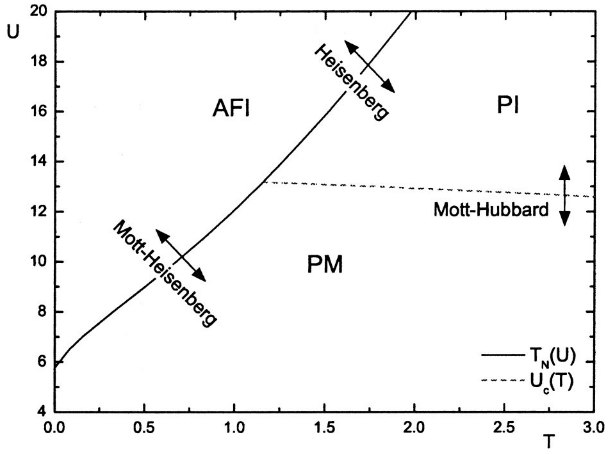

FIG. 8. The variety of transitions at $n=1$.

mainly due to the vanishing of a narrow coherent quasiparticle peak at the Fermi level as in the Gutzwiller approximation.[9] However, for an antiferromagnetic state on a bipartite lattice, this interpretation can be maintained within the DMFT only when frustration by an additional t' hopping is introduced.[9,37]

At half-filling, within the framework of the COM, we find three kinds of transitions: a Mott-Heisenberg transition (i.e., a transition between a paramagnetic metal and an antiferromagnetic insulator), driven mainly by the temperature at low values of the Coulomb interaction; a Mott-Hubbard transition (i.e., a transition between a paramagnetic metal and a paramagnetic insulator), almost insensitive to the temperature, at high values of the Coulomb interaction; and a Heisenberg transition (i.e., a transition between an antiferromagnet and a paramagnet), within the insulating phase, driven by the temperature at high values of the Coulomb interaction. Moreover, the central gap has two components depending on the value of the Coulomb interaction and the temperature: one due to the antiferromagnetic correlations (in the antiferromagnetic insulating phase), and another coming from the Mott-Hubbard mechanism (in the paramagnetic and antiferromagnetic insulating phases). In the Heisenberg transition the antiferromagnetic component of the central gap vanishes (i.e., the magnetization disappears and the lateral gaps close up), but the paramagnetic component remains finite. We have a finite critical value of the Coulomb interaction for the Mott-Hubbard transition, in contrast to what was found, for instance, by the Hubbard I approximation and the SDA. This fact allowed us to study the Mott-Heisenberg transition existing at lower values of the Coulomb interaction, that is obviously absent in any picture based on the approximations mentioned above (they do not have a Mott-Hubbard transition either). In Fig. 8 we summarize the transitions occurring at half-filling within a treatment of the Hubbard model in the framework of the COM.

The filling-controlled MIT is discontinuous at zero temperature. We have an antiferromagnetic insulator at $n=1$ and an antiferromagnetic metal at $n<1$, because the central gap is compensated for by the discontinuity in the chemical potential at $n=1$, and thus the Fermi level always lies inside the second antiferromagnetic band for $n<1$. This is exactly the same result as found in the usual mean-field approximation[43] and in the DMFT without frustration.[37] In the frustrated case with nonzero t' hopping, DMFT as well as quantum Monte Carlo studies additionally led to a U-controlled MIT inside the antiferromagnetic phase at $n=1$.[44,45]

Moving to finite temperature, the variation in the chemical potential, and thus in the overall band shift, is considerably moderated for higher values of T, whereas the central gap still remains large in comparison to kT. Therefore, we find a finite region around half-filling, where the Fermi level is still situated inside $\Delta_{\xi-\eta}$ and we thus have an antiferromagnetic phase of semiconductor type with very poor conductivity. When the Fermi level crosses the peak in the density of states at the upper edge of the second antiferromagnetic band, a huge jump in the number of carriers is observed, and we finally obtain an antiferromagnetic

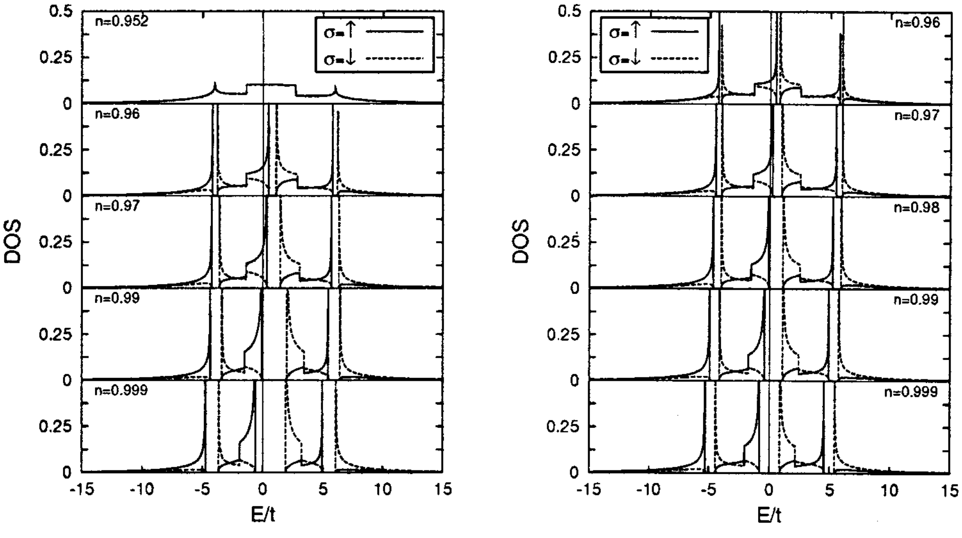

(a) (b)

FIG. 9. The sublattice density of states at $U=10t$ for various values of the particle density. The thin vertical line at $E=0$ denotes the position of the Fermi level E_F. (a) $kT=0.2$. (b) $kT=0.5t$.

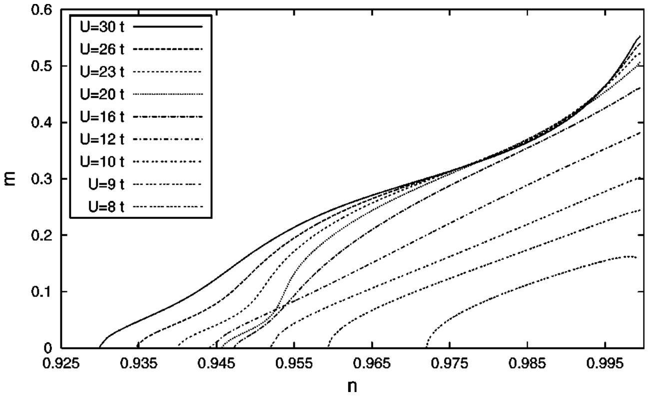

FIG. 10. The sublattice magnetization as a function of n at $kT=0.2t$.

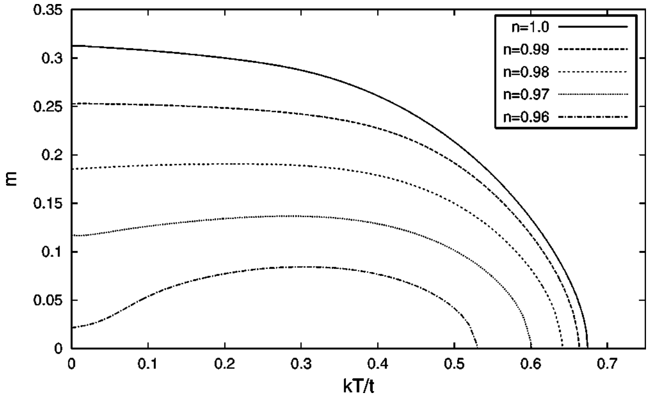

FIG. 11. The sublattice magnetization as a function of T and n at $U=10t$.

metal (see Fig. 9). Note that for the purely paramagnetic MIT such a filling controlled transition is not to be expected.

Comparing Figs.9(a) and 9(b) we see how the moderate evolution of the chemical potential as function of n leads to a larger extension of the insulating antiferromagnetic phase at higher temperatures.

The almost linear dependence of the central gap $\Delta_{\xi-\eta}$ on the Coulomb interaction U [cf. Fig. 7(a)] leads to a strong stabilization of the insulating antiferromagnetic phase at $n=1$. Near half-filling, however, this effect is compensated for by larger values of U due to the strong decay of the chemical potential when moving to lower particle densities. This decay of the chemical potential then leads to a large overall shift of the band structure toward higher energies, bringing the Fermi level close to the upper edge of the second antiferromagnetic band. After a small region, where the insulating phase is growing with U, this effect restricts the insulating antiferromagnetic phase to regions very close to half-filling for large values of U.

(c) Shape of the U-n phase diagram. For large values of the Coulomb interaction close to the critical value U_c, where antiferromagnetism is vanishing, the region of filling where the antiferromagnetic phase exists is enlarged by increasing U. Conversely, for intermediate values of U the antiferromagnetic region in doping shrinks. This can be explained by the closing of the Mott-Hubbard gap as a function of doping. When, at low values of U, no Mott-Hubbard gap is present, the magnetization and extension of the antiferromagnetic phase in n grow with growing U. After the opening of the Mott-Hubbard gap we find the system in a region where the Mott-Hubbard gap closes in the proximity of $n=1$, i.e., already within the antiferromagnetic phase. This leads to a shift of the Fermi level toward the middle of the second antiferromagnetic band, where majority and minority spins nearly have the same spectral weight, and thus to a considerable reduction of the staggered magnetization (cf. Fig. 10). For large values of U the Mott-Hubbard gap remains open within the whole region of doping, where the antiferromagnetic phase exists, and we again find an increasing stability of the antiferromagnetic phase with increasing Coulomb interaction.

(d) Heat magnetization. For small values of U we find an increasing of the stability in n of the antiferromagnetic phase by increasing temperature. In the same manner, when n is close to the phase boundary, the magnetization itself first increases with increasing T and then goes down to zero, as shown in Fig. 11. This so-called heat magnetization has its explanation in a strong change in the spectral weights of the spin subsystems by increasing temperature, whereas the Mott-Heisenberg gaps and the chemical potential are only subject to very small changes (see Fig. 12). At higher values of U, after the opening of the Mott-Hubbard gap, the stronger Coulomb interaction considerably stabilizes the antiferromagnetic state at low temperatures, and excludes the effect of heat magnetization.

C. Antiferromagnetic state of the 3D Hubbard model

The antiferromagnetic phase of the 3D Hubbard model is very similar to the one observed in two dimensions. The shape and main features of the phase diagrams (Figs. 13 and

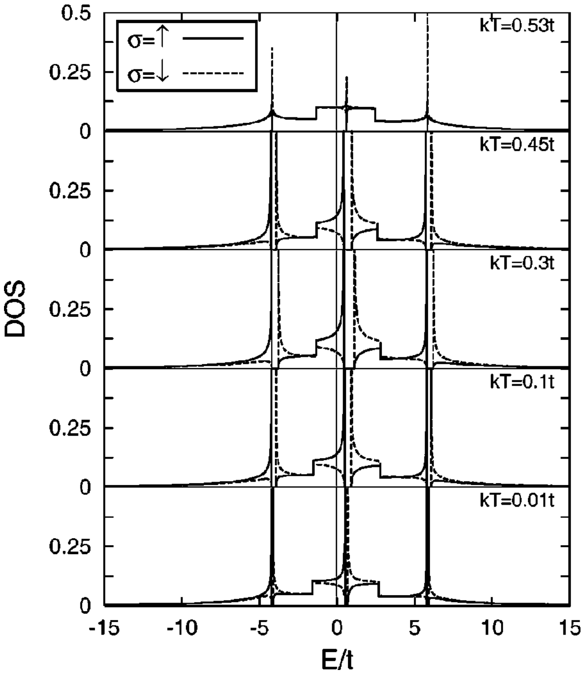

FIG. 12. The sublattice density of states for $U=10t$ and $n=0.96$.

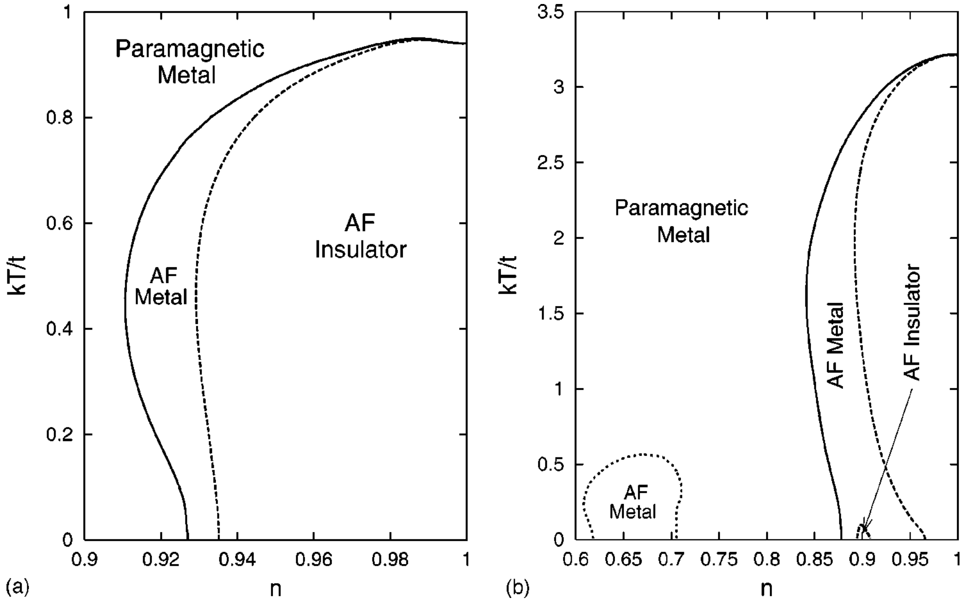

FIG. 13. The n-T phase diagram for the 3D Hubbard model. (a) Physical phase diagram at $U=10t$. (b) Complete phase diagram at $U=23t$.

14) remain unchanged (i.e., the MIT within the antiferromagnetic phase, the finite critical Coulomb interaction for the vanishing of the antiferromagnetic phase at half-filling, the favoring of the insulating state at high temperatures, and low values of the Coulomb interaction and the heat magnetization). Furthermore, as in the 2D case, all these properties can be explained by analyzing the density of states and the energy spectra.

The higher coordination number of the 3D model reduces the fluctuations, and leads to a greater stability of the antiferromagnetic phase as a function of the external parameters T, n, and U. Comparing the extension in n of our antiferromagnetic phase with the one found within the SDA for a fcc lattice,[26] the former is restricted to a much smaller region in doping.

The greater stability of the antiferromagnetic phase shows, within the range of physically relevant values of the parameter U, that the metallic antiferromagnetic phase extends to much lower values of n [cf. Figs. 13(b) and 14(b)] than might be expected from the phase diagrams in Figs. 13(a) and 14(a). For higher values of the Coulomb interaction, up to $U=30t$, this additional antiferromagnetic region is separated by the antiferromagnetic phase near half-filling by a paramagnetic region.

The form of the sublattice magnetization as a function of n for different values of the Coulomb interaction is given in Fig. 15. This result indicates that the two antiferromagnetic regions in the complete phase diagrams of Figs. 13 and 14 are actually two parts of a single antiferromagnetic solution, which are only connected at rather high values of U. We will discuss the nature of this ''tail'' in more detail in Sec. V, in the context of an analysis of the extended Hubbard model. Here we only remark that the separation of the two antiferromagnetic phase regions by a paramagnetic one is due to the closing of the Mott-Hubbard gap near $n=1$. This leads to a strong suppression of magnetization, as described in Sec.

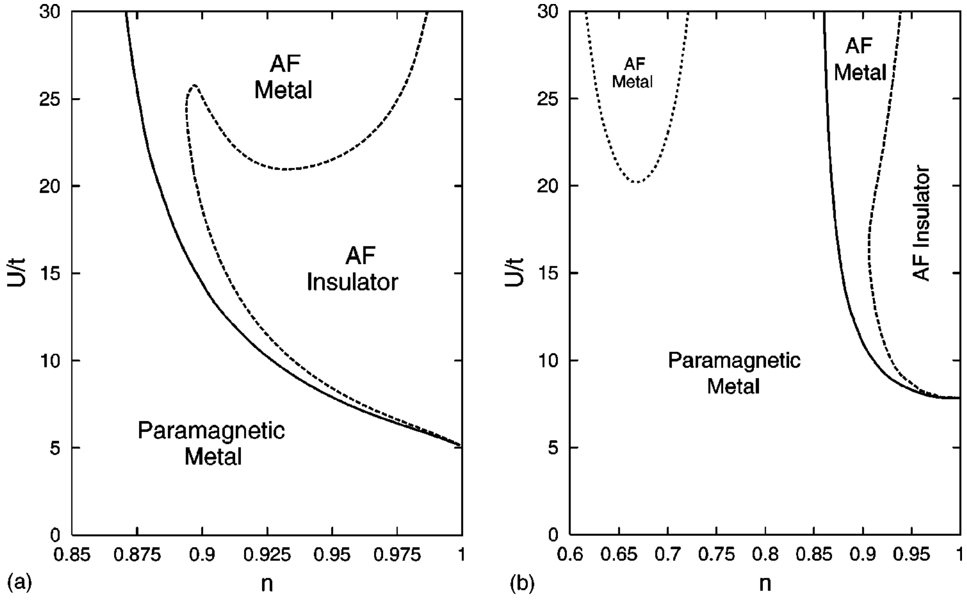

FIG. 14. The U-n phase diagram for the 3D Hubbard model. (a) Physical phase diagram at $kT=0.01t$. (b) Complete phase diagram at $kT=0.5t$.

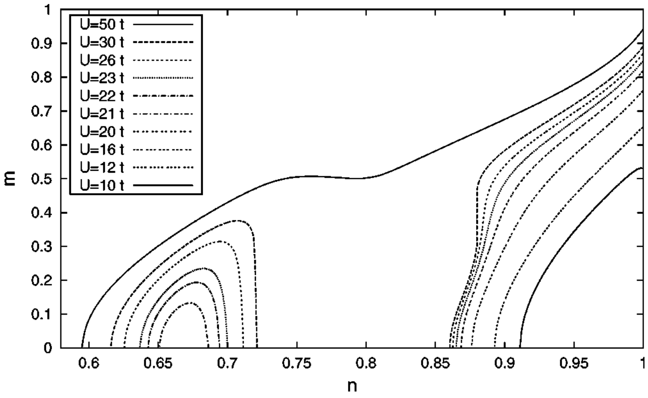

FIG. 15. The sublattice magnetization as a function of n at $kT=0.5t$ for different values of the Coulomb interaction.

IV B 2 c for the 2D case. The ‘‘antiferromagnetic tail,’’ which can be considered as an artifact of the employed approximation, is also present in the 2D case, but only appears at values of the Coulomb interaction $U\approx 100t$.

As we already mentioned in Sec. IV B 2, this ‘‘tail’’ at lower particle densities could be energetically ruled out by other phases with magnetic or spatial ordering.

Finally, in Fig. 16, we show the evolution of the sublattice density of states by changing the Coulomb interaction. We note a broader structure in comparison to the 2D model. As shown in Fig. 16(a), the transitions from metallic- to semiconductor-type antiferromagnetic states are related to the interplay between the global band shift and the evolution of the central gap. This explains the form of the insulating antiferromagnetic phase in Fig. 13(a).

V. EXTENDED HUBBARD MODEL

A. Model

In this section we study the antiferromagnetic solution of the *extended Hubbard model* in two dimensions. The model is described by the Hamiltonian

$$H^{ext}=\sum_{ij;\sigma}(t_{ij}-\mu\delta_{ij})c_{\sigma}^{\dagger}(i)c_{\sigma}(j)+U\sum_{i}n_{\uparrow}(i)n_{\downarrow}(i)+\sum_{ij;\sigma\sigma'}V_{ij}n_{\sigma}(i)n_{\sigma'}(j), \tag{5.1}$$

with the nearest-neighbor Coulomb interaction

$$V_{ij}=2V\alpha_{ij}=2V\frac{1}{N}\sum_{\mathbf{k}}e^{i\mathbf{k}\cdot(\mathbf{R}_i-\mathbf{R}_j)}\alpha(\mathbf{k}). \tag{5.2}$$

We proceed along the guidelines given in Sec. III to obtain the antiferromagnetic state. The equation of motion for the fundamental spinor [Eq. (2.2)] is given by

$$i\frac{\partial}{\partial t}\Psi(i,t)=[\Psi(i,t),H^{ext}]=\begin{pmatrix}-\mu\xi_{\uparrow}(i,t)-4tc_{\uparrow}^{\alpha}(i,t)-4t\pi_{\uparrow}^{\alpha}(i,t)+4Vn^{\alpha}(i,t)\xi_{\uparrow}(i,t)\\ -\mu\eta_{\uparrow}(i,t)+U\eta_{\uparrow}(i,t)+4t\pi_{\uparrow}^{\alpha}(i,t)+4Vn^{\alpha}(i,t)\eta_{\uparrow}(i,t)\\ -\mu\xi_{\downarrow}(i,t)-4tc_{\downarrow}^{\alpha}(i,t)-4t\pi_{\downarrow}^{\alpha}(i,t)+4Vn^{\alpha}(i,t)\xi_{\downarrow}(i,t)\\ -\mu\eta_{\downarrow}(i,t)+U\eta_{\downarrow}(i,t)+4t\pi_{\downarrow}^{\alpha}(i,t)+4Vn^{\alpha}(i,t)\eta_{\downarrow}(i,t)\end{pmatrix}, \tag{5.3}$$

where $n^{\alpha}(i)=\Sigma_{j\sigma}\alpha_{ij}n_{\sigma}(j)$. The normalization matrix I takes exactly the form given in Eqs. (3.4) and (3.6). For the m matrix we obtain the same result as given in Eq. (3.7) without the terms coming from the t' hopping, which are described by the projections β_{ij}. The matrices $M_1,\ldots,M_4$ are built up from matrices $\hat{M}_1,\ldots,\hat{M}_4$, as in Eq. (3.8), and these latter have the forms

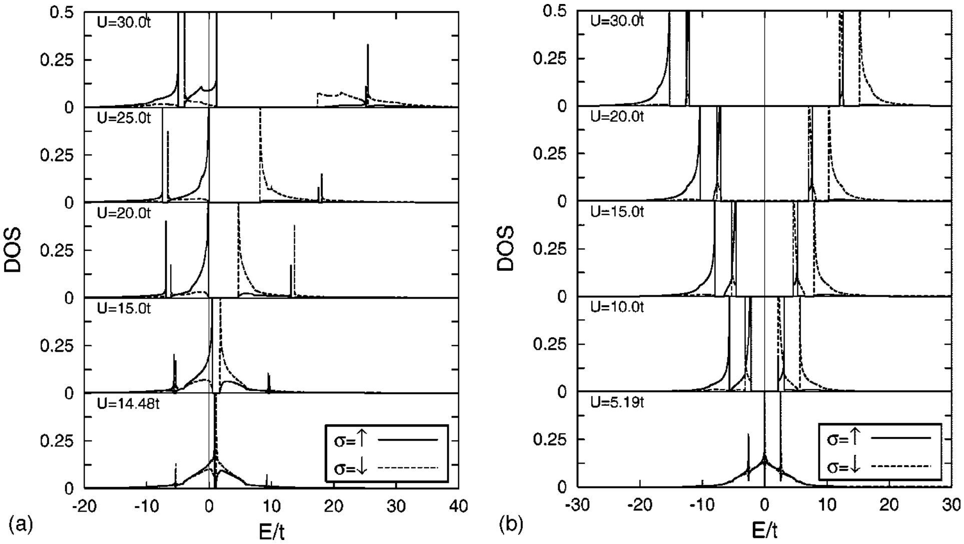

FIG. 16. The evolution of the sublattice density of states under a variation of the Coulomb interaction at $kT=0.01t$. The thin vertical line at $E=0$ denotes the position of the Fermi level E_F. (a) $n=0.9$. (b) $n=1.0$.

$$\hat{M}_1=\begin{pmatrix} -\mu\left(1-\frac{1}{2}n\right)-4t(\Delta_\downarrow^\alpha+\Delta_\uparrow^\alpha)+4V(n-\upsilon_\downarrow-\upsilon_\uparrow) & 4t(\Delta_\downarrow^\alpha+\Delta_\uparrow^\alpha) \\ 4t(\Delta_\downarrow^\alpha+\Delta_\uparrow^\alpha) & (U-\mu)\frac{1}{2}n-4t(\Delta_\downarrow^\alpha+\Delta_\uparrow^\alpha)+4V(\upsilon_\downarrow+\upsilon_\uparrow) \end{pmatrix},$$

$$\hat{M}_2=\begin{pmatrix} -\mu\frac{m}{2}-4t(\Delta_\downarrow^\alpha-\Delta_\uparrow^\alpha)+4V(-\upsilon_\downarrow+\upsilon_\uparrow) & 4t(\Delta_\downarrow^\alpha-\Delta_\uparrow^\alpha) \\ 4t(\Delta_\downarrow^\alpha-\Delta_\uparrow^\alpha) & -\frac{m}{2}(-\mu+U)-4t(\Delta_\downarrow^\alpha-\Delta_\uparrow^\alpha)+4V(\upsilon_\downarrow-\upsilon_\uparrow) \end{pmatrix}, \tag{5.4}$$

$$\hat{M}_3=\begin{pmatrix} -4t(1-n+p)+4V\lambda & -4t\left(\frac{1}{2}n-p\right)+4V(\nu_\uparrow+\nu_\downarrow) \\ -4t\left(\frac{1}{2}n-p\right)+4V(\nu_\uparrow+\nu_\downarrow) & -4tp+4V\kappa \end{pmatrix},$$

$$\hat{M}_4=\begin{pmatrix} 0 & -2tm+4V(\nu_\uparrow-\nu_\downarrow) \\ 2tm-4V(\nu_\uparrow-\nu_\downarrow) & 0 \end{pmatrix},$$

where we define the additional parameters

$$\lambda=\langle\xi_\sigma(i)\xi_\sigma^{\alpha\dagger}(i)\rangle=\langle\xi_{\bar{\sigma}}(i)\xi_{\bar{\sigma}}^{\alpha\dagger}(i)\rangle\quad\text{for}\ \ i\in\mathbf{A},$$

$$\nu_\sigma=\tfrac{1}{2}\langle\xi_\sigma(i)\,\eta_\sigma^{\alpha\dagger}(i)\rangle\quad\text{for}\ \ i\in\mathbf{A}, \tag{5.5}$$

$$\kappa=\langle\eta_\sigma(i)\,\eta_\sigma^{\alpha\dagger}(i)\rangle=\langle\eta_{\bar{\sigma}}(i)\,\eta_{\bar{\sigma}}^{\alpha\dagger}(i)\rangle\quad\text{for}\ \ i\in\mathbf{A},$$

$$\upsilon_\sigma=\tfrac{1}{2}\langle n^\alpha(i)n_\sigma(i)\rangle\quad\text{for}\ \ i\in\mathbf{A}.$$

We remark that the parameters λ and κ are not spin dependent because of the requirement for the m matrix to be real, and the additional symmetry constraint in assumption III.1.3. Furthermore, parameters Δ_σ^α can be expressed through parameters from Eq. (5.5) as

$$\Delta_\sigma^\alpha=\tfrac{1}{2}\lambda+\nu_\sigma-\nu_{\bar{\sigma}}-\tfrac{1}{2}\kappa. \tag{5.6}$$

The single-particle retarded Green's functions are calculated as in Eqs. (3.17) and (3.19), omitting the parts corresponding to the t' hopping. The parameters in Eq. (5.4) can then be calculated self-consistently by means of the correlation functions [Eqs. (3.21)]. The parameters m and μ are calculated as in Eq. (3.22a). The parameters λ, ν_σ, and κ are directly related to the single-particle retarded Green's functions by

$$\lambda=C_{11}^{AB\tilde{\alpha}}(\tilde{\mathbf{R}}_i),$$

$$\nu_\uparrow=\frac{1}{2}C_{12}^{AB\tilde{\alpha}}(\tilde{\mathbf{R}}_i),$$

$$\nu_\downarrow=\frac{1}{2}C_{12}^{BA\tilde{\alpha}}(\tilde{\mathbf{R}}_i), \tag{5.7}$$

$$\kappa=C_{22}^{AB\tilde{\alpha}}(\tilde{\mathbf{R}}_i),$$

and the parameters p and υ_σ, which derive from higher-order correlation functions, are used as in Eq. (3.22c) to satisfy the algebraic relations corresponding to the Pauli principle on the level of thermal equilibrium states:

$$C_{12}^{AA}(\tilde{\mathbf{R}}_i)=0,$$

$$C_{12}^{BB}(\tilde{\mathbf{R}}_i)=0,$$

$$C_{11}^{AA}(\tilde{\mathbf{R}}_i)=C_{11}^{BB}(\tilde{\mathbf{R}}_i).$$

Again, all the self-consistent equations are coupled.

B. Antiferromagnetic state of the 2D extended Hubbard model

The phase diagram corresponding to the antiferromagnetic thermal equilibrium state, obtained as a solution of the self-consistent equations (5.7), (3.22a), and (3.22c), is shown in Fig. 17 where we take a fixed ratio $U/V=5$. Again, the antiferromagnetic phase always has a lower free energy with respect to the paramagnetic phase, and the phase transition is always of second order.

The antiferromagnetic thermal equilibrium state fulfills the particle-hole symmetry. In addition, the main qualitative features of the antiferromagnetic states for the simple Hubbard model in two and three dimensions can also be found in the extended Hubbard model. There is a critical value of the Coulomb interaction, for which the antiferromagnetic phase disappears and a metal insulator transition occurs.

The phenomenon of heat magnetization is more pronounced than in the simple Hubbard model, and the occurrence of a tail in the antiferromagnetic solution is observed down to rather low values of U, where they can even join for higher temperatures. This leads to paramagnetic inclusions

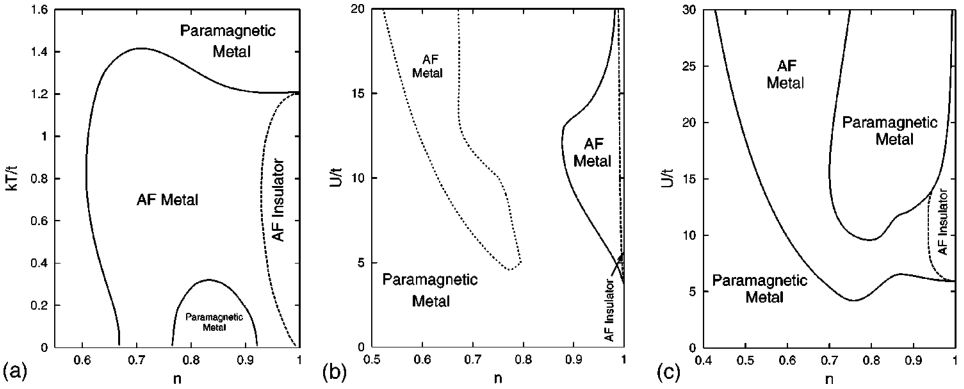

FIG. 17. The phase diagrams for the extended Hubbard model with $V=U/5$. (a) The n-T phase diagram at $U=8t$. (b) The U-n phase digram at $kT=0.01t$. (c) The U-n phae diagram at $kT=0.4t$.

within the antiferromagnetic phase. For higher values of U the antiferromagnetic phase is reduced to a very narrow region near half-filling.

The band structure turns out to be somehow different from the one found for the simple Hubbard model. The presence of the intersite Coulomb interaction leads to a large overlap of the antiferromagnetic bands, such that the opening of the Mott-Heisenberg gap at the crossing points cannot split the lower and upper Hubbard bands in most parts of the antiferromagnetic phase region. The sublattice density of states for the extended Hubbard model is thus mainly characterized by a single central gap, which is the superposition of the Mott-Heisenberg and the Mott-Hubbard gap (cf. Fig. 18).

The part of the antiferromagnetic phase at lower particle density is always characterized by this overlap of the antiferromagnetic subbands emerging from the lower and upper Hubbard bands, respectively. The absence of the Mott-Heisenberg gap within the Hubbard subbands reduces the number of peaks in the density of states to four: two peaks are due to the central gap, and two peaks are reminiscent of the van Hove singularity in each Hubbard band[46] (cf. Fig. 18).

In Fig. 19 we plot the sublattice magnetization as a function of the particle density for various values of the Coulomb interaction U, showing the separation of the antiferromagnetic phase by a paramagnetic region for high as well as low values of U.

The intersite Coulomb interaction V considerably reduces the magnetization and stability of the antiferromagnetic state, i.e., its extension in n, as can be seen from Fig. 20. The reduction of the magnetization also suppresses the separation of the two parts of the antiferromagnetic states. However, the suppression of antiferromagnetism by the intersite Coulomb interaction is much smaller than the one found in the treatment of the simple Hubbard model.

VI. CONCLUSIONS

Among the variety of analytical methods developed in the last decades to deal with strongly correlated electron systems, the COM has been rather successful in describing the properties of many correlated systems.[14,15,19,28,40,47] To add another piece to the puzzle constituted by the phase diagram of the Hubbard model, here we investigated the antiferromagnetic phase characterized by a staggered magnetization. A fully self-consistent treatment, respecting the symmetry constrains emerging from the Pauli principle, was presented for the Hubbard model in two and three dimensions and the two-dimensional extended Hubbard model.

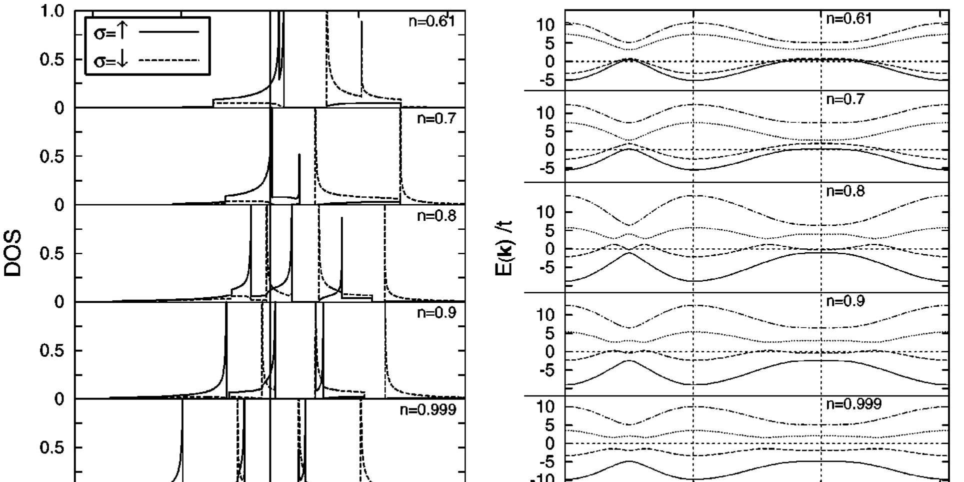

FIG. 18. Sublattice density of states and band structure at $kT=0.4t$ and with $V=U/5$; the thin vertical line at $E=0$ denotes the position of the Fermi level E_F. (a) Sublattice density of states for $U=9.5t$. (b) Band structure on the chemical lattice for $U=9.5t$.

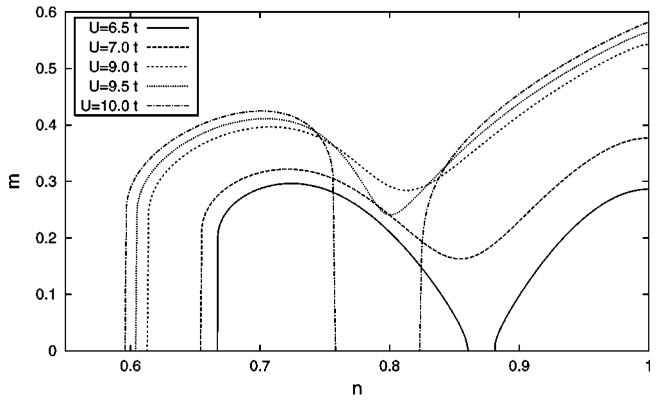

FIG. 19. Sublattice magnetization for different values of the Coulomb interaction at $kT = 0.4t$, with $V = U/5$.

The antiferromagnetic phases of the three systems, when compared to the corresponding paramagnetic phases, lead to a phase transition of the second order. In all cases the antiferromagnetic states have lower free energy. Furthermore, the antiferromagnetic states of all the models show the following properties.

(a) The presence of three kinds of transitions (Mott-Hubbard, Mott-Heisenberg, and Heisenberg) at half-filling in the plane T-U.

(b) The existence of two components in the antiferromagnetic gap (one due to the antiferromagnetic correlations, and another coming from the Mott-Hubbard mechanism).

(c) A finite critical value of the Coulomb interaction for the Mott-Hubbard and Mott-Heisenberg transitions.

(d) The antiferromagnetic phase is stable only in a very narrow region around half-filling, showing a strong reduction of the Néel temperature with doping.

(e) A metal-insulator transition, driven by the temperature, takes place within the antiferromagnetic phase; at half-filling and higher temperatures, this transition coincides with the paramagnetic-antiferromagnetic one.

(f) Away from half-filling, a metal-insulator transition driven by the doping is observed. This transition has the following properties: at zero temperature it is discontinuous, and connects an antiferromagnetic metal and an antiferromagnetic insulator; at finite temperature it connects the antiferromagnetic metal to an antiferromagnetic state of semiconductor type.

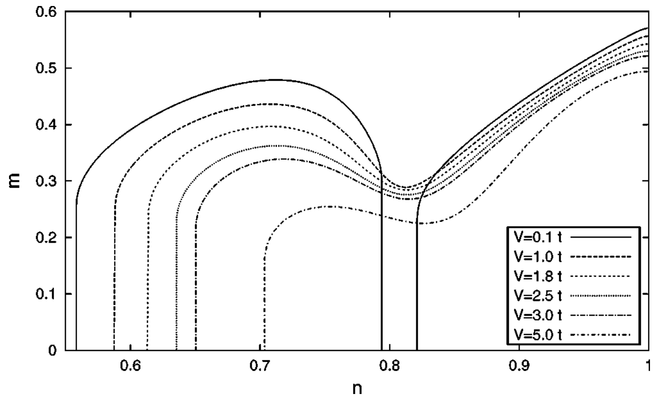

FIG. 20. Sublattice magnetization as a function of the particle density for different values of the intersite Coulomb interaction V, with $U = 9t$ and $kT = 0.4t$.

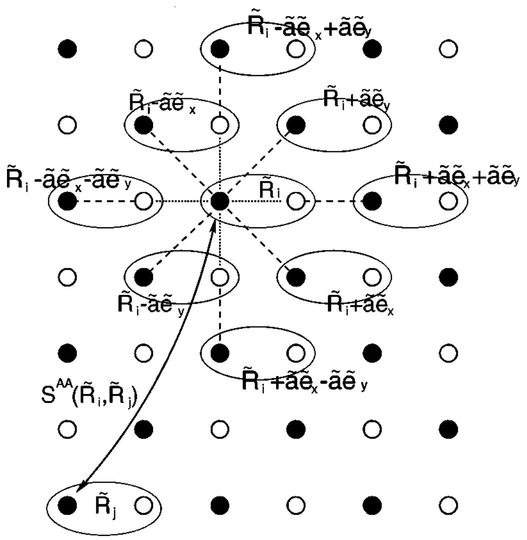

FIG. 21. The definition of the translationally invariant Green's function S^{AA}.

All these properties emerge from very strong correlations, and are not usually found by approximations of mean-field type. They could be explained by analyzing the electronic density of states and the energy spectra.

Finally, we want to point out that a thermodynamical study of the Hubbard model within the framework of the two-pole approximation by means of the COM is far from being completed. Besides the normal phase and the antiferromagnetic phase, a detailed analysis of superconducting,[48] ferromagnetic,[30] charge-ordered, and other phases with more complex magnetic and charge ordering has to be completed or undertaken, and these analyses should finally combine to give the complete phase diagram of the Hubbard model under this approach.

ACKNOWLEDGMENTS

This work was partially supported by the *Studienstiftung des deutschen Volkes*. One of the authors (R.M.) wants to thank Professor F. Mancini and the *Dipartimento di Fisica ''E.R. Caianiello''* at the University of Salerno for the hospitality and the motivating atmosphere during the period he stayed at the Institute. Furthermore, we want to thank Professor W. Nolting and Dr. V. Turkowski for helpful discussions.

APPENDIX A: CALCULATION OF THE GREEN'S FUNCTIONS FOR THE T-T'-U MODEL

On the magnetic lattice defined in Fig. 1, we can define the translationally invariant Green's functions $S^{AA}(\tilde{\mathbf{R}}_i,\tilde{\mathbf{R}}_j,t)$, $S^{AB}(\tilde{\mathbf{R}}_i,\tilde{\mathbf{R}}_j,t)$, $S^{BA}(\tilde{\mathbf{R}}_i,\tilde{\mathbf{R}}_j,t)$, and $S^{BB}(\tilde{\mathbf{R}}_i,\tilde{\mathbf{R}}_j,t)$ connecting two points $\tilde{\mathbf{R}}_i$ and $\tilde{\mathbf{R}}_j$ of the magnetic lattice. Their definition and the corresponding equations of motion are illustrated in Fig. 21 for the translational invariant Green's function S^{AA}. By means of a Fourier transform on the magnetic lattice,

$$\begin{aligned} S^{XY}(\tilde{\mathbf{R}}_i,\tilde{\mathbf{R}}_j,t)&=S^{XY}(\tilde{\mathbf{R}}_i-\tilde{\mathbf{R}}_j,t)\\ &=\frac{i}{2\pi}\left(\frac{\tilde{a}^2}{(2\pi)^2}\right)^2\int d\omega\; e^{-i\omega t}\\ &\quad\times\int_{\Omega_{\tilde{B}}}d^2\tilde{k}\; e^{i\tilde{\mathbf{k}}\cdot(\tilde{\mathbf{R}}_i-\tilde{\mathbf{R}}_j)}S^{XY}(\tilde{\mathbf{k}},\omega),\\ &\qquad X,Y\in\{\mathbf{A},\mathbf{B}\}, \end{aligned}\tag{A1}$$

the equations of motion for the translationally invariant Green's functions take the forms

$$\begin{aligned} \omega S^{AA}(\tilde{\mathbf{k}},\omega)&=[I^{(n)}+I^{(m)}]+([\varepsilon^{(1)}+\varepsilon^{(3)}]\\ &\quad+\tilde{\beta}(\tilde{\mathbf{k}})[\varepsilon^{(5)}+\varepsilon^{(6)}])S^{AA}(\tilde{\mathbf{k}},\omega)\\ &\quad+[\tilde{\alpha}(\tilde{\mathbf{k}})]^*[\varepsilon^{(2)}+\varepsilon^{(4)}]S^{BA}(\tilde{\mathbf{k}},\omega), \end{aligned}$$

$$\begin{aligned} \omega S^{AB}(\tilde{\mathbf{k}},\omega)&=([\varepsilon^{(1)}+\varepsilon^{(3)}]+\tilde{\beta}(\tilde{\mathbf{k}})[\varepsilon^{(5)}+\varepsilon^{(6)}])S^{AB}(\tilde{\mathbf{k}},\omega)\\ &\quad+[\tilde{\alpha}(\tilde{\mathbf{k}})]^*[\varepsilon^{(2)}+\varepsilon^{(4)}]S^{BB}(\tilde{\mathbf{k}},\omega), \end{aligned}$$

$$\begin{aligned} \omega S^{BA}(\tilde{\mathbf{k}},\omega)&=([\varepsilon^{(1)}-\varepsilon^{(3)}]+\tilde{\beta}(\tilde{\mathbf{k}})[\varepsilon^{(5)}-\varepsilon^{(6)}])S^{BA}(\tilde{\mathbf{k}},\omega)\\ &\quad+\tilde{\alpha}(\tilde{\mathbf{k}})[\varepsilon^{(2)}-\varepsilon^{(4)}]S^{AA}(\tilde{\mathbf{k}},\omega), \end{aligned}\tag{A2}$$

$$\begin{aligned} \omega S^{BB}(\tilde{\mathbf{k}},\omega)&=[I^{(n)}-I^{(m)}]+([\varepsilon^{(1)}-\varepsilon^{(3)}]\\ &\quad+\tilde{\beta}(\tilde{\mathbf{k}})[\varepsilon^{(5)}-\varepsilon^{(6)}])S^{BB}(\tilde{\mathbf{k}},\omega)\\ &\quad+\tilde{\alpha}(\tilde{\mathbf{k}})[\varepsilon^{(2)}-\varepsilon^{(4)}]S^{AB}(\tilde{\mathbf{k}},\omega), \end{aligned}$$

where we used the projections on the magnetic lattice $\tilde{\alpha}(\tilde{\mathbf{k}})=\frac{1}{4}[1+e^{i\tilde{k}_x\tilde{a}}+e^{i\tilde{k}_y\tilde{a}}+e^{i(\tilde{k}_x\tilde{a}+\tilde{k}_y\tilde{a})}]$ and $\tilde{\beta}(\tilde{\mathbf{k}})=\frac{1}{3}[4|\tilde{\alpha}(\tilde{\mathbf{k}})|^2-1]$ from Eq. (B3). Expressions (3.17) and (3.22) are obtained from Eqs. (A2) by lengthy but straightforward algebraic manipulations.

APPENDIX B: EXPLICIT EXPRESSIONS FOR GREEN'S FUNCTIONS OF THE ANTIFERROMAGNETIC EQUILIBRIUM STATE

For $X,Y\in\{\mathbf{A},\mathbf{B}\}$, the coefficients A^{XY}, B^{XY}, and C^{XY} occurring in expression (3.17) of the Green's functions, take the explicit forms

$$\begin{aligned} A^{AA}&=-\mathcal{E}_1^+-\mathcal{E}_2^+\mathcal{E}_1^-\frac{1}{\mathcal{E}_2^+}-\tilde{\beta}(\tilde{\mathbf{k}})\left[\mathcal{E}_3^++\mathcal{E}_2^+\mathcal{E}_3^-\frac{1}{\mathcal{E}_2^+}\right],\\ B^{AA}&=\mathcal{E}_2^+\mathcal{E}_1^-\frac{1}{\mathcal{E}_2^+}\mathcal{E}_1^++\tilde{\beta}(\tilde{\mathbf{k}})\left[\mathcal{E}_2^+\mathcal{E}_3^-\frac{1}{\mathcal{E}_2^+}\mathcal{E}_1^+\mathcal{E}_2^+\mathcal{E}_1^-\frac{1}{\mathcal{E}_2^+}\mathcal{E}_3^+\right]\\ &\quad+[\tilde{\beta}(\tilde{\mathbf{k}})]^2\mathcal{E}_2^+\mathcal{E}_3^-\frac{1}{\mathcal{E}_2^+}\mathcal{E}_3^+|\tilde{\alpha}(\tilde{\mathbf{k}})|^2\mathcal{E}_2^+\mathcal{E}_2^-,\\ C^{AA}&=I^{(n)}+I^{(m)},\\ D^{AA}&=-[\mathcal{E}_2^+\mathcal{E}_1^-+\tilde{\beta}(\tilde{\mathbf{k}})\mathcal{E}_2^+\mathcal{E}_3^-]\frac{1}{\mathcal{E}_2^+}[I^{(n)}+I^{(m)}],\\ A^{BB}&=-\mathcal{E}_1^--\mathcal{E}_2^-\mathcal{E}_1^+\frac{1}{\mathcal{E}_2^-}-\tilde{\beta}(\tilde{\mathbf{k}})\left[\mathcal{E}_3^-+\mathcal{E}_2^-\mathcal{E}_3^+\frac{1}{\mathcal{E}_2^-}\right],\\ B^{BB}&=\mathcal{E}_2^-\mathcal{E}_1^+\frac{1}{\mathcal{E}_2^-}\mathcal{E}_1^-+\tilde{\beta}(\tilde{\mathbf{k}})\left[\mathcal{E}_2^-\mathcal{E}_3^+\frac{1}{\mathcal{E}_2^-}\mathcal{E}_1^-+\mathcal{E}_2^-\mathcal{E}_1^+\frac{1}{\mathcal{E}_2^-}\mathcal{E}_3^-\right]\\ &\quad+[\tilde{\beta}(\tilde{\mathbf{k}})]^2\mathcal{E}_2^-\mathcal{E}_3^+\frac{1}{\mathcal{E}_2^-}\mathcal{E}_3^--|\tilde{\alpha}(\tilde{\mathbf{k}})|^2\mathcal{E}_2^-\mathcal{E}_2^+,\\ C^{BB}&=I^{(n)}-I^{(m)},\\ D^{BB}&=-[\mathcal{E}_2^-\mathcal{E}_1^++\tilde{\beta}(\tilde{\mathbf{k}})\mathcal{E}_2^-\mathcal{E}_3^+]\frac{1}{\mathcal{E}_2^-}[I^{(n)}-I^{(m)}]\\ A^{AB}&=A^{AA},\\ B^{AB}&=B^{AA},\\ C^{AB}&=0,\\ D^{AB}&=[\tilde{\alpha}(\tilde{\mathbf{k}})]^*\mathcal{E}_2^+[I^{(n)}-I^{(m)}],\\ A^{BA}&=A^{BB},\\ B^{BA}&=B^{BB},\\ C^{BA}&=0,\\ D^{BA}&=\tilde{\alpha}(\tilde{\mathbf{k}})\mathcal{E}_2^-[I^{(n)}+I^{(m)}]. \end{aligned}\tag{B1}$$

To abbreviate the notation we used the following definitions:

$$\begin{aligned} \mathcal{E}_1^+&=\varepsilon^{(1)}+\varepsilon^{(3)},\quad \mathcal{E}_1^-=\varepsilon^{(1)}-\varepsilon^{(3)},\\ \mathcal{E}_2^+&=\varepsilon^{(2)}+\varepsilon^{(4)},\quad \mathcal{E}_2^-=\varepsilon^{(2)}-\varepsilon^{(4)},\\ \mathcal{E}_3^+&=\varepsilon^{(5)}+\varepsilon^{(6)},\quad \mathcal{E}_3^-=\varepsilon^{(5)}-\varepsilon^{(6)}. \end{aligned}\tag{B2}$$

Furthermore, we used the convention that $\cos(\mathbf{Q}\cdot\mathbf{R}_i)$ takes positive values on the sublattice **A**, and we note that the projections on the nearest neighbors and on the next- and next-next-nearest neighbors according to the spherical approximation are given on the magnetic lattice by the expressions

$$\tilde{\alpha}(\tilde{\mathbf{k}})=\tfrac{1}{4}\left(1+e^{i\tilde{k}_x\tilde{a}}+e^{i\tilde{k}_y\tilde{a}}+e^{i(\tilde{k}_x\tilde{a}+\tilde{k}_y\tilde{a})}\right),$$

$$\tilde{\beta}(\tilde{\mathbf{k}})=\tfrac{1}{6}\left(e^{i\tilde{k}_x\tilde{a}}+e^{-i\tilde{k}_x\tilde{a}}+e^{i\tilde{k}_y\tilde{a}}+e^{-i\tilde{k}_y\tilde{a}}\right),+\tfrac{1}{12}\left(e^{i(\tilde{k}_x\tilde{a}+\tilde{k}_y\tilde{a})}+e^{-i(\tilde{k}_x\tilde{a}+\tilde{k}_y\tilde{a})}+e^{i(\tilde{k}_x\tilde{a}-\tilde{k}_y\tilde{a})}+e^{-i(\tilde{k}_x\tilde{a}-\tilde{k}_y\tilde{a})}\right). \tag{B3}$$

---

*Email address: avella@sa.infn.it

[1] J. Hubbard, Proc. R. Soc. London, Ser. A **276**, 238 (1963); **277**, 237 (1964); **281**, 401 (1964); **285**, 542 (1965); P. W. Anderson, Phys. Rev. **115**, 115 (1959).

[2] Y. Nagaoka, Phys. Rev. **147**, 392 (1966).

[3] H. Tasaki, J. Phys.: Condens. Matter (Paris) **10**, 4353 (1998).

[4] H. Tasaki, Prog. Theor. Phys. **99**, 489 (1998).

[5] F. Gebhard, *The Mott Metal-Insulator Transition: Models and Methods* (Springer, Berlin, 1997).

[6] J. Bednorz and K. Müller, Z. Phys. B: Condens. Matter **64**, 189 (1986).

[7] P. W. Anderson, Science **235**, 1196 (1987).

[8] E. Lieb, in *Proceedings of the XIth International Congress of Mathematical Physics* (International Press, Cambridge, MA, 1995), p. 392.

[9] A. Georges, G. Kotliar, W. Krauth, and M. J. Rozenberg, Rev. Mod. Phys. **68**, 13 (1996).

[10] L. M. Roth, Phys. Rev. **184**, 451 (1969).

[11] O. K. Kalashnikov and E. S. Fradkin, Phys. Status Solidi B **59**, 9 (1973).

[12] W. Nolting, Z. Phys. **255**, 25 (1972).

[13] A. J. Fedro *et al.*, Phys. Rev. B **46**, 14 785 (1992).

[14] S. Ishihara *et al.*, Phys. Rev. B **49**, 1350 (1994).

[15] F. Mancini, S. Marra, and H. Matsumoto, Physica C **244**, 49 (1995); **250**, 184 (1995); **252**, 361 (1995).

[16] P. Fulde, *Electron Correlations in Molecules and Solids*, 3rd ed. (Springer-Verlag, Berlin, 1995).

[17] H. Mori, Prog. Theor. Phys. **33**, 423 (1965); **34**, 399 (1965).

[18] R. Zwanzig, in *Lectures in Theoretical Physics* (Interscience, New York, 1961).

[19] H. Matsumoto, T. Saikawa, and F. Mancini, Phys. Rev. B **54**, 14 445 (1996); H. Matsumoto and F. Mancini, *ibid.* **55**, 2095 (1997).

[20] F. Mancini and A. Avella, cond-mat/0006377 (unpublished).

[21] F. Mancini and A. Avella, Condens. Matter Phys. **1**, 11 (1998).

[22] F. Mancini, D. Villani, and H. Matsumoto, Phys. Rev. B **57**, 6145 (1998); A. Avella, F. Mancini, and D. Villani, Solid State Commun. **108**, 723 (1998); A. Avella, F. Mancini, and D. Villani, Phys. Lett. A **240**, 235 (1998); F. Mancini, H. Matsumoto, and D. Villani, J. Phys. Stud. **4**, 474 (1999).

[23] A. Avella, F. Mancini, and M. M. Sánchez, Europhys. Lett. **44**, 328 (1998).

[24] W. Nolting and W. Borgel, Phys. Rev. B **39**, 6962 (1989).

[25] S. Bei der Kellen, W. Nolting, and G. Borstel, Phys. Rev. B **42**, 447 (1990).

[26] T. Herrmann and W. Nolting, J. Magn. Magn. Mater. **170**, 253 (1997).

[27] F. Mancini, Phys. Lett. A **249**, 231 (1998).

[28] A. Avella *et al.*, Int. J. Mod. Phys. B **12**, 81 (1998).

[29] E. Dagotto, Rev. Mod. Phys. **66**, 763 (1994).

[30] A. Avella, F. Mancini, and R. Münzner, Physica B **281-282**, 857 (2000).

[31] B. Chattopadhyay and D. Gaitonde, Phys. Rev. B **55**, 15 364 (1997).

[32] W. Zhang, M. Avignon, and K. Bennemann, Phys. Rev. B **45**, 12 478 (1992).

[33] W. Zhang and K. Bennemann, Phys. Rev. B **45**, 12 487 (1992).

[34] J. E. Hirsch, Phys. Rev. B **31**, 4403 (1985).

[35] A. Oleś and J. Spałek, Z. Phys. B: Condens. Matter **44**, 177 (1981).

[36] U. Trapper, H. Fehske, and D. Ihle, Physica C **282-287**, 1779 (1997).

[37] M. Jarrell and T. Pruschke, Z. Phys. B: Condens. Matter **90**, 187 (1993).

[38] R. Münzner, A. Avella, and F. Mancini, Physica B **284-288**, 1577 (2000).

[39] E. Dagotto *et al.*, Phys. Rev. B **45**, 10 741 (1992).

[40] F. Mancini, Europhys. Lett. **50**, 229 (2000).

[41] P. W. Anderson, Solid State Phys. **14**, 99 (1963).

[42] K. A. Chao, J. Spalek, and A. M. Oles, J. Phys. C **10**, L271 (1977).

[43] M. Imada, A. Fujimori, and Y. Tokura, Rev. Mod. Phys. **70**, 1039 (1998).

[44] D. Duffy and A. Moreo, Phys. Rev. B **55**, R676 (1997).

[45] R. Chitra and G. Kotliar, Phys. Rev. Lett. **83**, 2386 (1999).

[46] A. Avella, F. Mancini, D. Villani, and H. Matsumoto, Physica C **282-287**, 1759 (1997).

[47] F. Mancini, S. Marra, A. Allega, and H. Matsumoto, in *Superconductivity and Strongly Correlated Electron Systems* (World Scientific, Singapore, 1994), p. 271; D. Villani, E. Lange, A. Avella, and G. Kotliar, Phys. Rev. Lett. **85**, 804 (2000).

[48] T. Di Matteo, F. Mancini, and S. Marra, Condens. Matter Phys. **8**, 109 (1996); A. Avella, F. Mancini, H. Matsumoto, and D. Villani, Physica C **282-287**, 1757 (1997); T. Stanescu, I. Martin, and P. Phillips, Phys. Rev. B **62**, 4300 (2000).